IEEE Access
Multidisciplinary | Rapid Review | Open Access Journal

Received 1 July 2024, accepted 23 July 2024, date of publication 29 July 2024, date of current version 6 August 2024.

Digital Object Identifier 10.1109/ACCESS.2024.3434534

RESEARCH ARTICLE

Experimental Assessment of a Dual Super-Twisting Control Technique of Variable-Speed Multi-Rotor Wind Turbine Systems

HABIB BENBOUHENNI[1], MOURAD YESSEF[2], NICU BIZON[3], (Senior Member, IEEE), BADRE BOSSOUFI[2], AND THAMER A. H. ALGHAMDI[4,5]

[1]Department of Electrical and Electronics Engineering, Nisantasi University, 34398 Istanbul, Turkey
[2]LIMAS Laboratory, SMBA University, Fes 30000, Morocco
[3]The National University of Science and Technology POLITEHNICA Bucharest, Pitești University Centre, 110040 Pitești, Romania
[4]Electrical Engineering Department, Al-Baha University, Al Bahah 65779, Saudi Arabia
[5]Wolfson Centre for Magnetics, School of Engineering, Cardiff University, CF24 3AA Cardiff, U.K.

Corresponding authors: Habib Benbouhenni (habib.benbouenni@nisantasi.edu.tr) and Thamer A. H. Alghamdi (Alghamdit1@cardiff.ac.uk)

ABSTRACT Experimental work using Hardware-in-the-loop simulation is performed in this article for a power system based on multi-rotor wind energy for power generation. Power is generated using a doubly-fed induction generator (DFIG), where the suggested approach to regulate the energy is different from the direct power command (DPC) in terms of idea and structure, even though the same equations are used to estimate the powers. Two parallel super-twisting controls are used to control the power, and modified space vector modulation (MSVM) is used to operate the rotor side converter. The designed command is unrelated to the system's mathematical model and uses only a few gains, which makes it an effective and distinctive effectiveness compared to the DPC based on the super-twisting controller (DPC-STC). Also, simplicity, robustness, and ease of application are the most notable characteristics of the suggested command. Moreover, an uncontrolled grid-side converter was used to demonstrate the efficacy and competence of the suggested command in ameliorating the features of the designed power system. The suggested command was first verified in MATLAB, and the results were confirmed using experimental work, where Hardware-in-the-loop using the dSPACE 1104 was used for this purpose. In this work, the results obtained with the DPC-STC technique were compared in terms of undulations and oscillation minimization ratio, total harmonic distortion (THD) of stream, and steady-state error (SSE) value. The designed command minimized the THD of current with an efficiency of 45.94%, 46.95%, and 45.93% in the first test, second test, and third test, respectively. Also, the active power undulations were minimized compared to the DPC-STC by58.33%, 45.60%, and 44.88% in the first test, second test, and third test, respectively. The SSE of reactive power was also reduced by 68%, 71.32%, and 70.80% in the first test, second test, and third test, respectively. These ratios indicate the effectiveness, ability, and efficiency of the suggested command to ameliorate the efficiency of the power system.

INDEX TERMS Doubly-fed induction generator, super-twisting controls, direct power command, multi-rotor wind energy.

NOMENCLATURE

DFIG	Double-Fed Induction generator.
DTC	Direct torque control.
PWM	Pulse width modulation.
FL	Fuzzy logic.
MSVM	Modified space vector modulation.
STC	Super-twisting control.
HC	Hysteresis comparator.
Ps	Active power.
Qs	Reactive power.

The associate editor coordinating the review of this manuscript and approving it for publication was Ehab Elsayed Elattar.

DSTC	Dual super-twisting control.
DPC	Direct power control.
PI	Proportional-integral.
MPPT	Maximum power point tracking.
SMC	Sliding mode control.
MRWT	Multi-rotor wind turbine.
SSE	Steady-state error.
THD	Total harmonic distortion.
FOC	Field-oriented control.
LT	Lookup table.
ANFIS	Adaptive-network-based fuzzy inference system.

I. INTRODUCTION

In the last years, the direct power control (DPC) approach has become one of the most prominent aproaches in the area of command, that have appeared in recent years as a genuine solution among the suggested solutions for regulating and regulate machines. The direct torque control (DTC) and this approach are extremely similar, as it has the same principle and idea, and the difference between them consists in the references used or the regulated quantities [1]. In the DPC, both the reactive (Qs) and active power (Ps) are regulated, while in the DTC, the flux and torque are regulated directly without the utilization of internal loops [2]. Simplicity, robustness, low cost, and few gains usedare among the characteristics that makes DPC famous compared to both vector command and field-oriented control (FOC) [3]. The DPC strategy was used to control a photovoltaic system based on the filtration [4] and control system of the doubly-fed induction generator (DFIG) [5]. Also, it was used to control the power of the synchronous generator [6], as its use greatly improved the dynamic response of these energy systems.However, some drawbacks limit the use of this method, as the current quality is low and there are high fluctuations at the level of both the Ps and Qs as a result of using the hysteresis comparator (HC) [7]. Also, a lookup table (LT) is used to produce command pulses in the IGBTs of the converter, which results in an electric current of non-constant frequency, which is undesirable [8]. Several genuine solutions have been designed to ameliorate the advantages and defeat the cons and defects of the DPC, such as the use of neural networks (NNs) [9], synergetic control (SC) [10], fuzzy logic (FL) [11], genetic algorithm [12], sliding mode controller (SMC) [13], backstepping command [14], super-twisting control (STC) [15], and fractional-order control [16]. Using these techniques leads to ameliorate the advantages and significantly reduce the Qs and Ps fluctuations. Also, the DPC based on these methods becomes difficult to achieve, expensive more complex.

STC approach is among the non-linear strategies designed to surpass some real problems of the SMC, which is distinguished by high competence, easy to apply, and can be used in many fields such as controlling machines and renewable energy sources [17]. It was proposed in the work [18] to use the STC to overcome the problems and defects of the DPC of DFIG strategy, where a control of the STC was used to command the power. The STC approach was used to determine the voltage reference values based on the power error, where the voltage reference values are used to generate operating pulses for the rotor side converter (RSC) of DFIG. The DPC-STC is a modified strategy of the traditional DPC, where robustness, high competence, and efficiency are the most important features of this approach. The negative of this strategy lies in the use of estimation of capabilities and the presence of a significant number of gains. In [19], the author used the STC strategy with a neural controller in order to ameliorate the competence of the DFIG-based wind turbine system. Using the neural STC strategy to control power led to a higher number of gains compared to the conventional strategy that relies on the use of a proportional-integral (PI) regulator. Also, the neural STC strategy is difficult and expensive to implement compared to PI control. This proposed technique is verified using processor in the loop (PIL) based experimental setup carried out in MATLAB/Simulink. Results showed that the neural STC strategy significantly reduced power ripples, total harmonic distortion (THD) of current, overshoot, and steady-state error (SSE) compared to the PI control. In terms of response time (RT), using the neural STC strategy led to an unsatisfactory time compared to PI control, which is negative.

Super-twisting HC is a solution that has been proposed to overcome the cons of the DPC of DFIG-based multi-rotor wind turbine (MRWT) system in [20]. In this work, the STC strategy was used to replace conventional regulators (HCs) for DPC, where the author kept using ST to produce the pulses needed to operate the RSC of DFIG-MRWT system. This approach has several advantages, including simplicity, performance, high durability, and ease of implementation. This proposed strategy was implemented and the algorithm was validated using the MATLAB, where numerical and graphical results showed that the proposed strategy significantly reduced ripples, overshoot, and SSE of DFIG power compared to the DPC. But in terms of RT, the designed strategy provided an unsatisfactory RT compared to the DPC strategy. Also, it is noted that the proposed approach is affected by changing machine parameters, which is a negative matter that contributes to a decrease in the quality of current and power. According to the work done in [21], the STC provided unsatisfactory results compared to the SC approach of DFIG. First, the author conducted a comparative study between the two strategies in terms of simplicity, ease of use, number of gains, durability, competence, and ease of completion. Secondly, the two strategies were verified using the MATLAB, where two strategies were used to improve the performance of the DPC of DFIG strategy. Numerical results were extracted for the various tests performed, and the completed comparison showed that the STC has an unsatisfactory performance compared to the SC approach, and this is highlighted by the calculated reduction ratios.

Given the importance of the STC, as it is considered an appropriate solution, several solutions have been designed to improve its characteristics and raise performance. The proposed solutions to overcome the problems of the STC are different, as most of them depend on introducing other strategies into the STC approach (merging) in order to overcome the defects. In [22], the author proposed a new strategy for the STC to improve performance and increase durability. This approach lies in the multivariate adaptive STC method, where the adaptation scheme is based on a two-layer structure. Also, it does not require knowledge of the upper bounds for identical perturbations. It is possible to adapt both gains to impose a second-order SMC while avoiding over estimation of the disturbance, which is important for mitigating the unwanted effects of chatter by exploiting information extracted from the equivalent command. In the work [23], the author uses a simplified structure of the STC approach as a convenient and effective solution to overcome the problems and drawbacks of the STC. This proposed strategy was used to overcome the drawbacks of the filter-based photovoltaic system. The results highlight the effectiveness of the proposed approach in improving the characteristics of the studied energy system compared to the conventional approach, and this is shown by the graphical and numerical results. Also, the proposed approach gave a value for the THD of current that is much better than several existing controls, which is a positive thing that highlights the high performance of this solution, making it one of the most important solutions that can be relied upon in the field of control in the future. To overcome the shortcomings of the STC, the author in the work [24] relied on fractional calculus. He relied on this strategy because of its characteristics such as simplicity and high durability. The proposed STC approach was used to improve the characteristics of the indirect FOC approach of asynchronous generator-based wind turbine. Accordingly, the proposed control is characterized by complexity, a large number of gains, difficulty of implementation, and reliance on capacity estimation, which makes the control affected by changing the machine parameters. However, despite these drawbacks, the designed control provided very satisfactory results compared to the conventional approach, and this is shown by the results from the MATLAB. Fractional-order proportional-integral STC is a solution that was proposed in the work [25] to improve the quality of current and power output from DFIG, where the MATLAB was used to implement, verify, and find out the robustness of the proposed solution compared to PI control. This designed solution has both positives and negatives, as its negatives lie in its complexity, expensiveness, large number of gains, and difficulty of implementation compared to the conventional approach. Its most prominent advantages are high performance, great durability, and efficiency, as the numerical results show these positive features of this proposed approach. Also, this proposed strategy provided very satisfactory results compared to several research works in terms of reducing the value of response time and the value of THD of current. The NN technique and STC were combined to overcome the problems of the DPC of DFIG-MRWT in [26], where simulation was used to implement the designed strategy. Using neural STC as an effective solution that significantly improved characteristics of the energy system in all tests performed compared to conventional PI-based command. This approach wasimplemented experimentally using Hardware-in-the-loop (HIL) simulation based on dSPACE 1104 in [27], where the author used two different forms of wind speed (WS) in order to study the behavior of the neural STC. The experimental results showed the high performance of this approach and the validity of the simulation. Also, it is noted that the energy ripples remain present and are not completely overcome, which is a negative thing. Neural-SC-STC techniques was adopted as a suitable and effective solution to overcome the problem of low power quality and current in the DFIG-MRWT system [28], as the author used this proposed approach to compensate for traditional regulators (PI). Relying on this proposed approach led to improving the values of THD of current, overshoot, power ripples, and SSE compared to the conventional approach, and this is shown by the numerical and graphical values obtained from the MATLAB under different working conditions for DFIG. The negatives of this proposed solution lie in the complexity, the number of internal layers and neurons for each layer needed to obtain good results, the large number of gains, and the difficulty of implementation. Also, its reliance on capacity estimation makes it give unsatisfactory results in terms of power quality and current. Another simple solution based on the use of the STC was implemented in the work [29], where this solution was used in order to overcome the disadvantages of the DPC approach of DFIG-MRWT system. This solution relies on the use of the dual STC (DSTC) technique in order to command the power, as this strategy was applied to the RSC of DFIG without the grid side converter (GSC). This solution was implemented using the MATLAB and experimental using HIL test, and several tests were used for this purpose. All test results confirm the effectiveness and performance of the DSTC approach in improving the characteristics of the studied energy system compared to the conventional approach, and this is what the calculated reduction ratios show.

In this work, dual STC is used to ameliorate the advantages and effectiveness of the DPC of DFIGs, where two STC regulators are used in parallel to regulate the Ps and the same applies to the Qs. So, the essential contribution of the study lies in proposing the DSTC technique as a suitable solution to reduce energy undulations and minimize the THD value of current. Moreover, the second contribution lies in the use of DPC-DSTC based on modified space vector modulation (MSVM) to regulate the RSC of DFIG-MRWT. To demonstrate the characteristic of the DPC-DSTC in ameliorating the system features, GSC is used using a diode, as the system becomes simpler and less expensive. The obtained method is featured by high efficiency and low Ps and Qs ripples

compared to the DPC. First, MATLAB was used to verify the robustness and effectiveness of the DPC-DSTC, comparing the competence to the DPC-STC in terms of minimizing fluctuations, THD value, robustness, SSE, and tracking the DFIG-MRWT power reference. Secondly, the third contribution of this study is the implementation of DPC-DSTC with HIL test (dSPACE 1104) using two different WS profiles and the comparison of the experimentally obtained results with the simulation results. Accordingly, the objectives achieved by this work can be defined in the following points:

- Overcoming the cons of the DPC of DFIG-MRWT;
- Experimental confirmation of a system based on MRWT;
- Significantly reduces current/power ripples;
- Significantly increases the robustness of DFIG-MRWT system;
- Improved THD value for current;
- Improved SSE and overshoot values.

The work has been divided into 5 different divisions. In the second division, an overview of the suggested approach represented by DSTC is given. The DPC-DSTC strategy is detailed in Section three. Graphical and numerical results are given in the Section IV, with three tests used for this purpose. In the fifth section, the proposed control is achieved experimentally using HIL test (dSPACE 1104), where a variable WS is used and the results are compared. The work is concluded with a set of conclusions that summarize the purpose of the work with reference to future work.

II. MRWT SYSTEM

The energy system based on MRWT is considered one of the most prominent energy systems that significantly reduces the phenomenon of global warming and protects the environment from pollution. The use of this energy system reduces the use of non-renewable sources such as gas and allows the costs of producing electrical energy to be significantly reduced. Also, relying on the energy system allows it to overcome the increasing demand for electrical energy, which makes it of great importance in the energy field. This studied energy system consists of an MRWT turbine, a DFIG generator, two inverters, and a network. To complete this energy system, it is necessary to provide mathematical modeling for each part. This mathematical modeling is used to simulate the system in MATLAB. In this studied energy system, a two-level inverter is used to achieve RSC and GSC, which is implemented using an uncontrolled inverter to simplify the system and reduce its total cost.

A. TWO-LEVEL INVERTER MODEL

Traditionally, the two-level inverter is considered the cornerstone of multi-level inverters, as it is characterized by simplicity, ease of control, and ease of implementation. In this inverter, six IGBT transistors are used. In order to control this inverter, the PWM or SVM strategy is used. Several other strategies can be relied upon to control this inverter, as complexity, simplicity, and ease of implementation are among the most prominent features of any approach that can be relied upon to command this inverter.

The mathematical model for this inverter is represented in Equation (1). This inverter was used to embody the RSC of DFIG, as this inverter was relied upon to simplify the system and reduce its costs.

$$\begin{bmatrix} V_a \\ V_b \\ V_c \end{bmatrix} = \frac{E}{6} \begin{bmatrix} 2 & -1 & -1 \\ -1 & 2 & -1 \\ -1 & -1 & 2 \end{bmatrix} \begin{bmatrix} F_1 \\ F_2 \\ F_3 \end{bmatrix} \tag{1}$$

where, V_a, V_b, and V_c are the three-phase voltages.

$F_1 = \mathrm{K}_1 + K'_1$, $F_2 = \mathrm{K}_2 + K'_2$, and $F_3 = \mathrm{K}_3 + K'_3$

K_1, K_2, and K_3 arethe top switch.

K'_1, K'_2, and K'_3 are the bottom switch.

$$F_1 = \begin{cases} 1 \textit{ when } K_1 \textit{ is closed and } K'_1 \textit{ is open} \\ -1 \textit{ when } K'_1 \textit{ is closed and } K_1 \textit{ is open} \end{cases}$$

$$F_2 = \begin{cases} 1 \textit{ when } K_2 \textit{ is closed and } K'_2 \textit{ is open} \\ -1 \textit{ when } K'_2 \textit{ is closed and } K_2 \textit{ is open} \end{cases}$$

$$F_3 = \begin{cases} 1 \textit{ when } K_3 \textit{ is closed and } K'_3 \textit{ is open} \\ -1 \textit{ when } K'_3 \textit{ is closed and } K_3 \textit{ is open} \end{cases}$$

B. DFIG MODEL

In the field of renewable energies, DFIG is considered one of the most prominent solutions that can be relied upon for generating electrical energy due to the characteristics that distinguish it from other generators. This generator converts energy gained from the air into electrical energy. This generator consists of two sections: a fixed section and a moving section. According to the work done in [22], conventional DFIG cannot operate under open-phase conditions. There are three-phase DFIG, which is considered more common, as well as five- [30], six- [31], and seven-phase DFIG [32], where the greater the number of phases, the greater the capacity and size of the DFIG. As is known, increasing the number of phases contributes significantly to increasing the torque value. But the negative of increasing the number of stages lies in the increase in the cost of the machine, its weight, and the difficulty of control. Compared to both synchronous generators and vernier permanent magnet machines (VPMM) [33], the power generated by DFIG can be controlled by feeding the rotor using two different inverters, which allows this generator to give greater efficiency in case of variable wind speed. Also, the stator part of DFIG is connected directly to the network without using an intermediary, which is not found in other generators. Compared to both synchronous generators and VPMM, DFIG is characterized by simplicity of control, low cost, high durability, low periodic maintenance, and slippage, which makes it one of the most reliable generators for generating electrical power. To find out the mathematical model of DFIG, the Park transform is used for this purpose. The mathematical model of DFIG is to give mathematical equations for both the mechanical and electrical sections of the machine, where Equation (2) represents the mechanical

section of the generator. This equation gives the evolution of speed as a function of torque.

$$\begin{cases} T_e = J \times \dfrac{d\Omega}{dt} + f \times \Omega + T_r \\ T_r = 1.5p \times \dfrac{M}{L_s}(-\Psi_{sd} \times I_{rq} + \Psi_{sq} \times I_{rd}) \end{cases} \tag{2}$$

Equation (3) shows the voltage and flux of the rotor section, where these two quantities are related to the current.

$$\begin{cases} V_{dr} = R_r I_{dr} - w_r \Psi_{qr} + \dfrac{d}{dt}\Psi_{dr} \\ \Psi_{dr} = L_r I_{dr} + M I_{ds} \\ V_{qr} = R_r I_{qr} + w_r \Psi_{dr} + \dfrac{d}{dt}\Psi_{qr} \\ \Psi_{qr} = M I_{qs} + L_r I_{qr} \end{cases} \tag{3}$$

The expressions for the voltage and flux of the stator section are represented in Equation (4).

$$\begin{cases} V_{qs} = R_s I_{qs} + w_s \Psi_{ds} + \dfrac{d}{dt}\Psi_{qs} \\ \Psi_{qs} = M I_{qr} + L_s I_{qs} \\ V_{ds} = R_s I_{ds} - w_s \Psi_{qs} + \dfrac{d}{dt}\Psi_{sd} \\ \Psi_{ds} = L_s I_{ds} + M I_{dr} \end{cases} \tag{4}$$

To calculate powers, Equation (5) can be used, where both current and voltage measurements are used for this purpose.

$$\begin{cases} P_s = 1.5 \times (V_{qs} \times I_{qs} + I_{ds} \times V_{ds}) \\ Q_s = 1.5 \times (-I_{qs} \times V_{ds} + V_{qs} \times I_{ds}) \end{cases} \tag{5}$$

C. MRWT MODEL

Traditionally, the energy generated by wind-using turbines depends on several factors such as the size of the turbine, the speed of the wind, and the distance of the turbines from each other. The use of traditional three-bladed turbines in order to obtain mechanical energy causes several problems and disadvantages, as these turbines are affected by the wind generated between the turbines in wind farms, which leads to a decrease in the energy yield of the wind farm. Also, in order to obtain greater energy, turbines with large dimensions must be used, which is difficult in terms of costs and implementation of the turbine on the ground. Therefore, researchers found the solution by using MRWT turbines. According to the work done in [34], the MRWT turbine provides more energy gained from the wind than the energy provided by the single-rotor turbine. Also, the rotational speed of the MRWT turbine is greater than the rotational speed of a normal turbine. In MRWT, several turbines can be used to form the mother turbine, whereas in our work the study is limited to using two turbines to form the MRWT turbine. So the torque and power resulting from MRWT are expressed by Equation (6).

$$\begin{cases} T = T_2 + T_1 \\ P = P_1 + P_2 \end{cases} \tag{6}$$

In Equation (7), the torque for each turbine is shown, where the torque value is related to the WS and the dimensions of each turbine. The larger the dimensions, the greater the torque value.

$$\begin{cases} T_2 = \dfrac{C_p}{2\lambda_2^3}\rho \cdot \pi \cdot R_2^5 \cdot w_2^2 \\ T_1 = \dfrac{C_p}{2\lambda_1^3}\rho \cdot \pi \cdot R_1^5 \cdot w_1^2 \end{cases} \tag{7}$$

The energy produced by the MRWT turbine is the sum of the energy of each turbine, where Equation (8) is used to express the energy produced by each turbine that makes up the MRWT. This energy output is also related to both the WS and the turbine dimensions.

$$\begin{cases} P_2 = \dfrac{C_p(\beta, \lambda)}{2}\rho \cdot S_2 \cdot w_2^3 \\ P_1 = \dfrac{C_p(\beta, \lambda)}{2}\rho \cdot S_1 \cdot w_1^3 \end{cases} \tag{8}$$

According to Equation (8), the power of each turbine is affected by a factor called the coefficient of power (Cp), where its value is less than 1. The power gained from the wind is greater in the case when this coefficient takes the value of 1. This factor is related to the pitch angle (β) and tip speed ratio (λ), where the Equation (9) expresses how to determine it.

$$C_p(\lambda, \beta) = 0.0068\lambda + 0.517\left(\frac{116}{\lambda_i} - 0.4\beta - 5\right)e^{\frac{-21}{\lambda_i}} \tag{9}$$

With:

$$\lambda_i = \frac{0.035}{\beta^3 + 1} + \frac{1}{0.08\beta + \lambda} \tag{10}$$

Equation (11) expresses the tip speed ratio of each turbine used to create the MRWT.

$$\begin{cases} \lambda_2 = \dfrac{w_2 \cdot R_2}{V_2} \\ \lambda_1 = \dfrac{w_1 \cdot R_1}{V_1} \end{cases} \tag{11}$$

In MRWT, each turbine has its own WS. The WS of the second turbine is affected by the first turbine. The latter's speed is the WS. According to the work done in [35], the WS of the second turbine is given by the following relationship:

$$V_2 = V_1\left(1 - \frac{1 - \sqrt{(1 - C_T)}}{2}\left(1 + \frac{2x}{\sqrt{1 + 4x^2}}\right)\right) \tag{12}$$

where, V_1 is the WS of second turbine, C_T is a constant gain ($C_T = 0.9$), V_2 is the WS of first turbine, and x is a distance between the both turbines. In this work, the value of x is estimated at 15 m because the power value of the turbine is 1.5 MW.

In order to control the MRWT turbine, the maximum power point tracking (MPPT) strategy is used for this purpose, as this approach was discussed in detail in the work [36].

III. MSVM TECHNIQUE

MSVM is one of the solutions proposed to replace the traditional SVM strategy for controlling inverters. This strategy is characterized by simplicity, inexpensiveness, easy to implement, and outstanding performance, which makes it one of the most suitable and reliable solutions for controlling reflectors. This strategy was discussed in detail in the work [37], where its positives and negatives were addressed. In the work [38], the author implemented the MSVM strategy for a two-level inverter experimentally using dSPACE. The experimental results were compared with both SVM and PWM, where the experimental results showed that the MSVM strategy is more efficient and performant than the SVM and PWM strategies. In this work, the MSVM strategy will be discussed for a two-level inverter that is used to feed the DFIG rotor, as it was relied upon due to the features that distinguish it and the results it provided in terms of the value of THD of the current compared to both SVM and PWM.

The principle of the MSVM strategy is determined in four steps:

- Step 1: Calculate Maximum of the power source;
- Step 2: Calculate Minimum of the power source;
- Step 3: Calculate the sum of Min (*Va*, *Vb*, and *Vc*) and Max(*Va*, *Vb*, and *Vc*);
- Step 4: Generation of pulse series *Sa, Sb,* and *Sc*.

According to the steps mentioned above, Figure 1 represents the MSVM approach used in this work to control the RSC of DFIG.

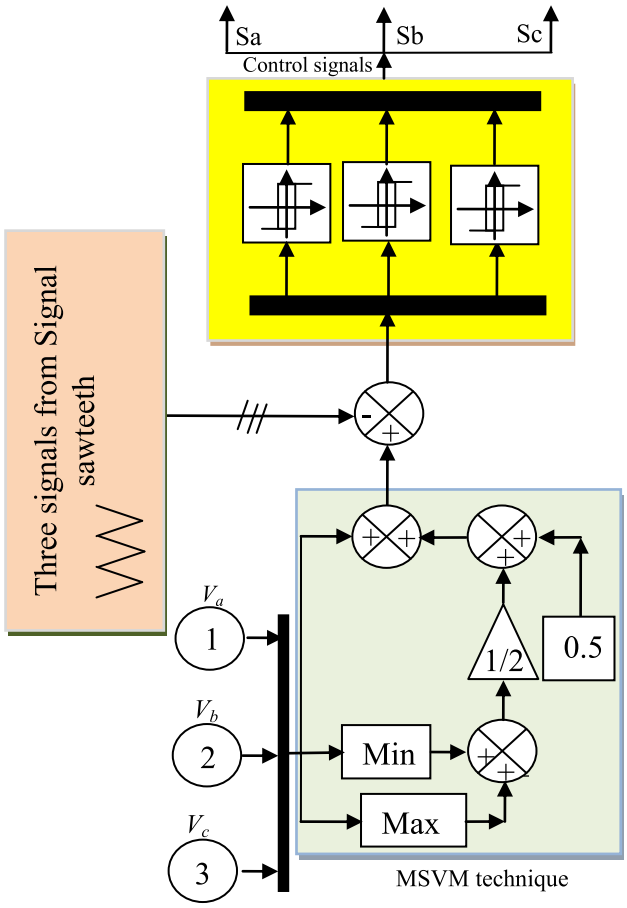

FIGURE 1. Two-level MSVM technique of RSC.

IV. DESIGNED STRATEGY

Traditionally, the DPC approach is considered one of the strategies that have a rapid, dynamic response, which makes it one of the most reliable solutions. Also, simplicity, low cost, and ease of implementation are among the most prominent characteristics that distinguish this approach from other controls. However, this approach has negatives that hinder its spread, as the most prominent of these negatives lie in the low durability in the event of a malfunction in the system, high energy fluctuations, the value of the THD of the stream, and the estimation of capabilities. Many solutions have been proposed to overcome these drawbacks, but the DSTC controller is considered one of the most important solutions that were presented in the work [29] to overcome these problems.

A. DSTC CONTROLLER

According to the work done in [39], the STC approach has positives and negatives, as the author in this work completed a comparison between the two strategies STC and SC of the DFIG-based MRWT system. The results obtained showed the superiority of the synergetic control strategy over the STC approach in terms of improving the system characteristics. Accordingly, the author of the work [29] believes that using the dual STC approach is one of the simplest and most reliable solutions, as two STC-type commands are used in parallel in order to overcome the defects and problems of the STC approach. This proposed solution does not require complex calculations or knowledge of the mathematical model of the system under study, which makes it one of the most prominent solutions that can be relied upon. According to the work [17], the expression for the STC regulator can be expressed by Equation (13).

$$Y(t) = K_1 |S|^r \, sign(S) + K_2 Sing(S) \tag{13}$$

where, K_2 and K_1 are the gains of the STC technique, S is the surface, and r is the exponent defined for the STC approach.

Based on the Equation (13) and according to the work done in [29], the DSTC approach can be expressed by the Equation (14).

$$y(t) = y_1(t) + y_2(t) \tag{14}$$

With:

$$y_1(t) = (K_1 |e_1|^{r_1} \, sign(e_1) + K_2 Sing(e_1)) \tag{15}$$

$$y_2(t) = (K_3 |e_2|^{r_2} \, sign(e_2) + K_4 Sing(e_2)) \tag{16}$$

where, e_1 and e_2 are the surface of the designed DSTC technique, r_1 and r_2 are theexponent defined for the DSTC technique. Figure 2 represents both the STC and DSTC approaches used in this work.

The traditional STC strategy is represented in Figure 2a and Figure 2b is a simple diagram of the DSTC technique.

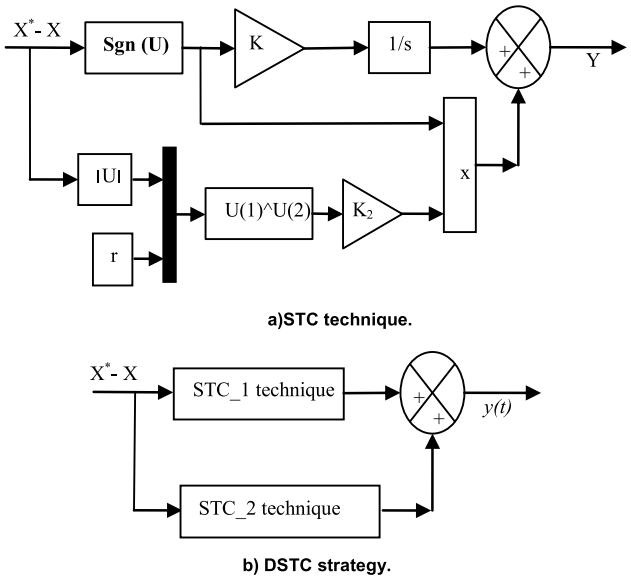

FIGURE 2. DSTC controller.

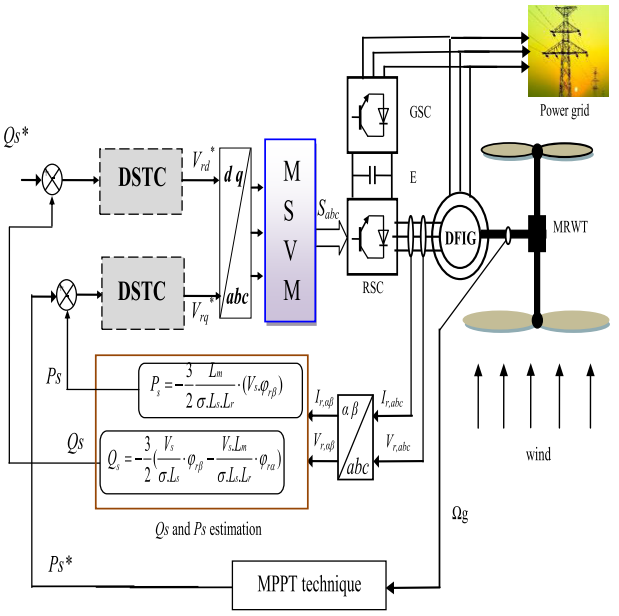

FIGURE 3. Proposed DPC-DSTC-MSVM of DFIG-MRWT.

Accordingly, from these forms, it is noted that these strategies are characterized by simplicity and ease of implementation, which is a positive thing.

In Table 1, a comparison is made between the two strategies DSTC and STC, where their similarities and differences are given.

TABLE 1. Comparison between the two strategies DSTC and STC.

	STC strategy	DSTC technique
Number of *e*	1	2
Number of *r*	1	2
Number of sign(u)	**2**	4
Number of gain	**2**	4
Using the mathematical model of the system	**No**	No
Ease of experimental implementation	Yes	Yes
Simplicity	Yes	No
Complexity	No	Yes
Performance	Medium	High
Robustness	Medium	High

B. DPC-DSTC-MSVM TECHNIQUE

Figure 3 represents the DPC-DSTC suggested using a two-level MSVM technique in this study for controlling the *Qs* and *Ps* of DFIG-MRWT. The DPC-DSTC-MSVM technique differs from the DPC technique in idea and principle, where the ST and HCs were dispensed with and replaced with both the two-level MSVM approach and two DSTC controllers. One of the most important features of the DPC-DSTC-MSVM is its robustness and high efficiency in minimizing *Ps* and *Qs* fluctuations. Also, the current quality is improved compared to the DPC strategies.

The DPC-DSTC-MSVM strategy has similarities with the traditional strategy, as these similarities lie in the use of the same controlled electrical quantities. Also, use the same estimating equations for capacities.

In the DPC-DSTC, two DSTC regulators were used to command the powers, where the outputs of these controllers are the voltage reference values. These voltage reference values are used to produce the operating pulses of the RSC of DFIG-MRWT. Therefore, the complexity, number of gains, and difficulty of completion can be considered among the most important disadvantages of this command compared to the DPC technique. However, the use of a DSTC regulator increases the solidity and performance of the studied DFIG-MRWT, as overcoming energy and stream fluctuations is one of the most prominent goals of this work.

The DPC-DSTC-MSVM technique in this paper uses the same estimation equations used in the DPC to estimate both the Qs and Ps. The Qs reference value can be set to 0 and the MPPT technique is used to calculate the Ps reference value.

To estimate the DFIG energy, the Equations (17) and (18) are used. In addition, we need to know the rotor flux, where the voltage and current are measured to know the flux.

Equation (19) is used to calculate the flux [9].

$$P_s = -\frac{3}{2}\frac{Lm.(Vs.\Psi_{r\beta})}{.Lr.\sigma.Ls} \tag{17}$$

$$Q_s = -\frac{3}{2}\left(-\frac{Vs.Lm}{\sigma.Ls.Lr}\cdot\Psi_{r\alpha} + \frac{Vs}{\sigma.Ls}\cdot\Psi_{r\beta}\right) \tag{18}$$

where, $\Psi_{r\beta}$ is the flux linkage of β-axis, Lm is the mutual inductance, $\Psi_{r\alpha}$ is the rotor flux linkage of α-axis.

$$\left|\overline{\Psi_s}\right| = \frac{\left|\overline{V_s}\right|}{w_s} \tag{19}$$

$$\sigma = 1 - \frac{M^2}{L_r\, L_s} \tag{20}$$

Equation (21) can be used to calculate the $\Psi_{s\beta}$ and $\Psi_{s\alpha}$. The angle between $\Psi_{s\beta}$ and $\Psi_{s\alpha}$ is given by Equation (22) [7], [9].

$$\begin{cases} \Psi_{s\alpha} = \int_0^t (-R_s\, I_{s\alpha} + V_{s\alpha})dt \\ \Psi_{s\beta} = \int_0^t (-R_s\, I_{s\beta} + V_{s\beta})dt \end{cases} \tag{21}$$

where, $V_{s\alpha}$ and $V_{s\beta}$ are the voltage linkage of $\alpha - \beta$ axis.

$$\theta_s = arctg(\frac{\Psi_{s\beta}}{\Psi_{s\alpha}}) \tag{22}$$

Equation (23) represents the flux in terms of $\Psi_{s\alpha}$ and $\Psi_{s\beta}$.

$$\Phi_s = \sqrt{\Psi_{s\alpha}^2 + \Psi_{s\beta}^2} \tag{23}$$

The two Equations (24) and (25) represent the estimation of the Qs and Ps using both the stator flux and the rotor flux.

$$P_s = -\frac{3}{2}\frac{Lm}{\sigma.Ls.Lr}\, w_s \left|\psi_s\right| |\psi_r| \sin(\lambda) \tag{24}$$

$$Q_s = -\frac{3}{2}\frac{ws}{\sigma.Ls} \left|\psi_s\right| (\frac{M}{L_r} |\psi_r| \cos(\lambda) - \left|\psi_s\right|) \tag{25}$$

Using Equations (14) to (16), the reference value for V_{dr} can be written according to Equation (26). The reference value for V_{qr} can also be written using Equation (29).

$$V_{dr}^* = y_1\,(t) + y_2\,(t) \tag{26}$$

With:

$$y_1\,(t) = (K_1\,|e_1|^{r_1}\, sign\,(e_1) + K_2 Sing(e_1)) \tag{27}$$

$$y_2\,(t) = (K_3\,|e_2|^{r_2}\, sign\,(e_2) + K_4 Sing(e_2)) \tag{28}$$

where, K_1, K_2, K_3, and K_4 are the gains of the DSTC controller of Qs of DFIG.

$$V_{qr}^* = y_3\,(t) + y_4\,(t) \tag{29}$$

With:

$$y_3\,(t) = (K_5\,|e_3|^{r_3}\, sign\,(e_3) + K_6 Sing(e_3)) \tag{30}$$

$$y_2\,(t) = (K_7\,|e_4|^{r_4}\, sign\,(e_4) + K_8 Sing(e_4)) \tag{31}$$

where, K_5, K_6, K_7, and K_8 are the gains of the DSTC controller of Ps of DFIG.

Figure4 represents the DPC-DSTC-MSVM strategy for controlling the Qs and Ps of the DFIG using the DSTC technique, where two DSTC technique are used. The purpose of using DSTC is to determine the reference values of both the $V_{r\alpha}$ and $V_{r\beta}$ from the Qs and Ps errors.

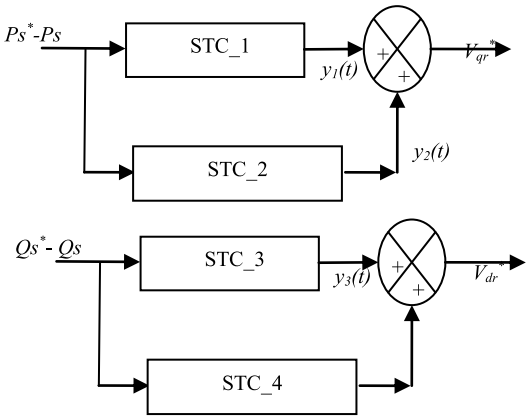

FIGURE 4. Proposed DSTC regulator of the P_S and Q_S.

V. SIMULATIONS RESULTS

To study the characteristic of the DPC-DSTC-MSVM technique compared to the DPC-STC techniques, the numerical simulation of the DFIG-based MRWT system was accomplished using MATLAB software. The parameter used in this work is the same as the parameters used in the work [15], [16], where a generator with a capacity of 1500 kW was used (See Appendix).

To study the performance of strategies, two different forms of WS are used, from which the necessary graphical and numerical results are extracted. The comparison between the approaches is made in terms of reference tracking, robustness, performance, reduction in RT, jitter, overshoot, and SSE of DFIG-MRWT power. Also, the two approaches are compared in terms of the THD of current.

A. TEST_1

In this first test, the effectiveness of the DPC-DSTC-MSVM is studied in comparison with the DPC-STC in terms of reference tracking. In this test, the WS was used in steps as shown in Fig. 5a.

From the system responses given in Figs. 5b and 5c for both techniques the Qs and Ps tracks the reference powers with fluctuations in both techniques. Active power follows the change in WS, and takes negative values. But the Qs is not affected by the change in WS, as it remains constant and equal to the value 0.

Fig. 5d represents the current change for the two controls. This current changes according to the change in WS, as its value increases and decreases as the WS increases and decreases. Also, the shape of this current is sinusoidal for both controls, with the DPC-DSTC-MSVM having an advantage in terms of fluctuations compared to the DPC-STC.

Figs. 5e and 5f represent the value of both the THD of current and the amplitude value of the fundamental signal (50Hz) for the two controls. From these two figures, the THD value was 1.48% and 0.80% for both the DPC-STC and the DPC-DSTC-MSVM, respectively. So, the DPC-DSTC-MSVM approach reduced the THD value by an estimated

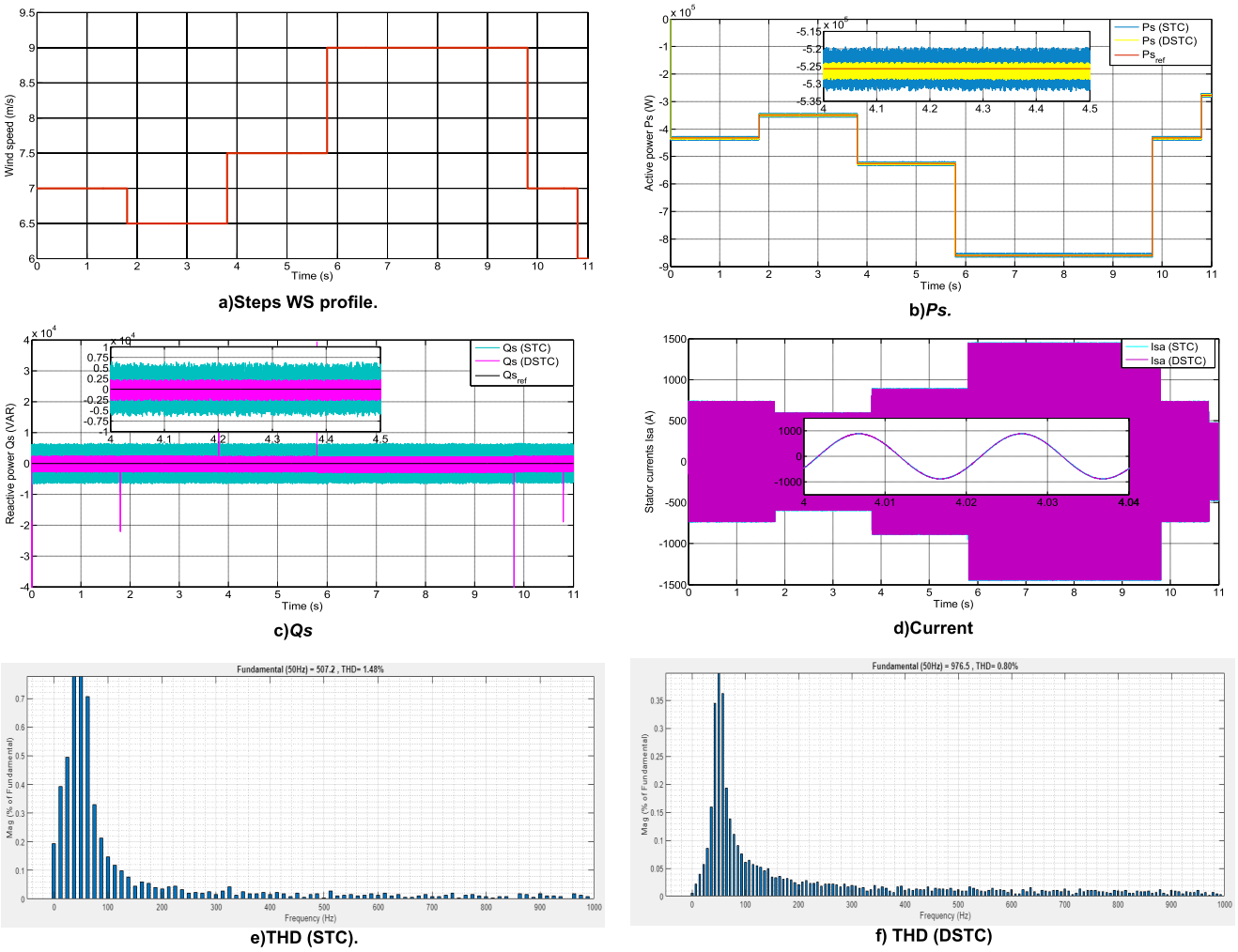

FIGURE 5. First test results.

45.94% compared to DPC-STC. On the other hand, the amplitude of the fundamental signal (50Hz) was 507.20 A and 976.5 A for both the DPC-STC and the designed technique, respectively. Through these values, the DPC-DSTC-MSVM reduced the value of this amplitude by an estimated ratio of 48.05%. These percentages indicate that the DPC-DSTC-MSVM has the ability to significantly improve the quality of the stream compared to the DPC-STC.

The numerical results of this test for the two controls are listed in Table 2, where values and reduction percentages are given for fluctuations, RT, overshoot, and SSE of DFIG power. Through this table, the strategy provided satisfactory results in terms of fluctuations, overshoot, and SSE compared to the DPC-STC. In the case of *Ps*, the DPC-DSTC-MSVM reduced the values of fluctuations, overshoot, and SSE by percentages estimated at 58.33%, 62.55%, and 65.51%, respectively, compared to the DPC-STC. In the case of *Qs*, these ratios were estimated at 69.29%, 51.49%, and 68% for fluctuations, overshoot, and SSE, respectively, compared to the DPC-STC. It is noted that these reduction rates

TABLE 2. The overshoot, response time, ripples and SSE ratios of the DFIG energy (Test 1).

		Ps (W)	*Qs* (VAR)
DPC-STC	Ripples	12000	12200
	Overshoot	2350	1340
	SSE	2175	1250
	Response time	0.45 ms	0.52 ms
DPC-DSTC	Ripples	5000	3750
	Overshoot	880	650
	SSE	750	400
	Response time	0.98 ms	0.89 ms
Improvement ratios	Ripples	58.33%	69.26%
	Overshoot	62.55%	51.49%
	SSE	65.51%	68%
	Response time	-54.08%	-51.57

are high, which indicates the high performance of the DPC-DSTC-MSVMin improving the characteristics of the studied energy system. However, it is noted from the table that DPC-DSTC-MSVM provided a response time to the capabilities

greater than the time provided by DPC-STC which is not satisfactory, as this negativity can be attributed to the method of choosing (calculating) the values of the designed command parameters. Therefore, the DPC-STC reduced the response time compared to DPC-DSTC-MSVM by percentages estimated at 54.08% and 51.57% for *Ps* and *Qs*, respectively.

B. TEST_2

This second test differs from the first test in terms of the form of WS change used to study the characteristics of the DPC-DSTC-MSVM. The WS used in this test is shown in Fig. 6a, where it is noted that the *Ps* continues to follow the reference well for the two commands, with its value increasing and decreasing as the WS increases and decreases (Fig. 6b). Also, this power continues to take negative values, as is the case in the first test, with fluctuations at the two control levels. These fluctuations are larger when using the DPC-STC compared to the DPC-DSTC-MSVM.

Fig. 6c represents the change in *Qs* for the two controls, where the same observations as in the first test are observed. This ability continues to follow the reference well even with the presence of fluctuations, as these fluctuations are low when using the DPC-DSTC-MSVM technique compared to the DPC-STC. Also, this power is not affected by changing WS, as its value remains constant throughout the simulation period and is equal to the value 0 VAR.

Fig. 6d represents the current change profile for the two commands. This current's value is related to the change in WS, as its value decreases and increases as the WS decreases and increases. This current has a sinusoidal shape for both commands, with the DPC-DSTC-MSVM technique having an advantage in terms of current quality compared to the DPC-STC.

The signal amplitude value of fundamental (50 Hz) and THD value of current for the two controls are represented in Figs. 6e and 6f. From these two figures, it is noted that the amplitude value was 504.1 A and 808.50 A for both the DPC-STC and the DPC-DSTC-MSVM, respectively. Therefore, the DPC-DSTC-MSVM strategy reduced the value of this amplitude by an estimated percentage of 37.64% compared to the DPC-STC. Also, the THD value was 1.64% and 0.87% for both the DPC-STC and the DPC-DSTC-MSVM, respectively. So, the designed strategy gave a value to THD much lower than the DPC-DTC, as it reduced its value by an estimated rate of 46.95%. These percentages indicate the efficiency and ability of the DPC-DSTC-MSVM to improve the quality of the stream compared to the DPC-STC.

Table 3 shows the numerical values with the reduction ratios for the second test, which are related to the variable WS. The values of fluctuations, SSE, and overshoot of DFIG power were low when using the DPC-DSTC-MSVM compared to the DPC-STC, which is a good thing. Accordingly, the DPC-DSTC-MSVM reduced the values of fluctuations, SSE, and overshoot of Ps by ratios estimated at 45.60%, 73.33%, and 70.83%, respectively, compared to

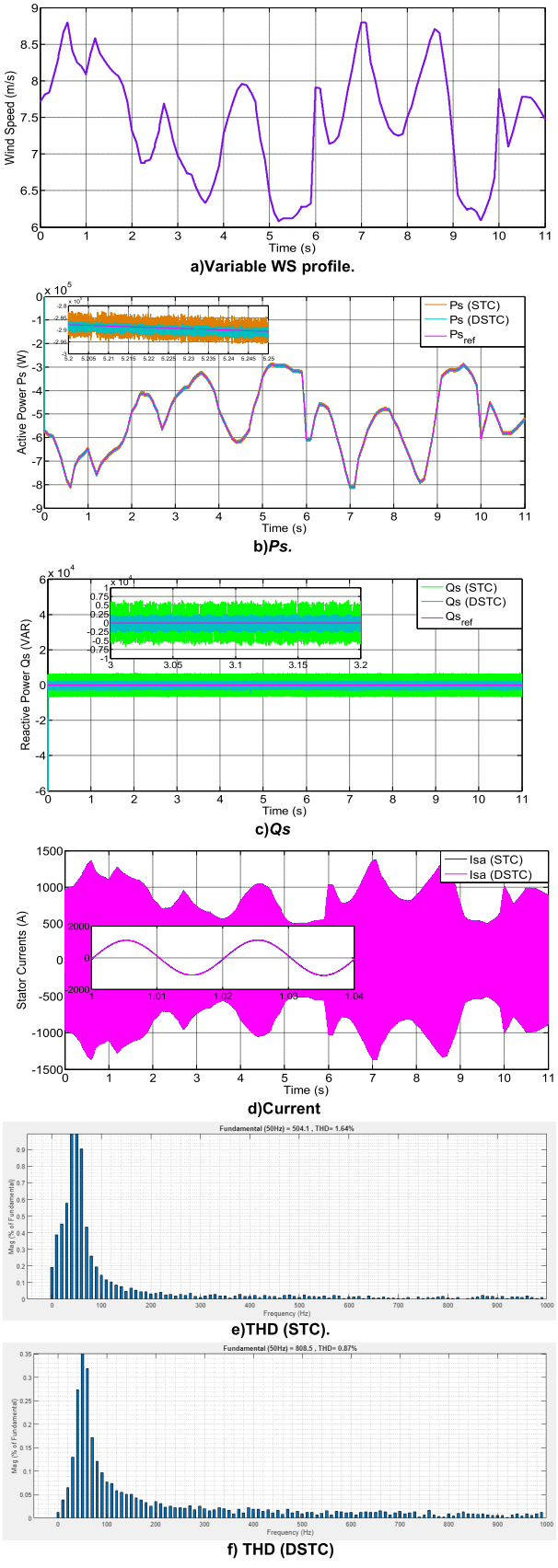

FIGURE 6. Second test results.

TABLE 3. The response time, overshoot, ripples and SSE ratios of the DFIG energy (Test 2).

		Ps (W)	*Qs* (VAR)
DPC-STC	Ripples	12500	11900
	Overshoot	2400	1400
	SSE	2250	1325
	RT	0.60 ms	0.75 ms
DPC-DSTC	Ripples	6800	4850
	Overshoot	700	520
	SSE	600	380
	RT	1.23 ms	1.45 ms
Improvement ratios	Ripples	45.60%	59.24%
	Overshoot	70.83%	62.85%
	SSE	73.33%	71.32%
	RT	-51.21%	-48.27%

the DPC-STC. Also, the values of fluctuations, SSE, and overshoot of Qs were reduced by ratios estimated at 59.24%, 71.32%, and 62.85%, respectively, compared to the DPC-STC.

The RT to capabilities was better when using the DPC-STC compared to the DPC-DSTC-MSVM. Therefore, the RT to the capabilities is negative for the strategy designed in this test. This time was reduced by ratios estimated at 48.27% and 51.21% for Qs and Ps, respectively. Grey wolf optimization can be used in the future to overcome the problem of response time to capabilities in the DPC-DSTC-MSVM.

In Table 4, the change in the values of both THD and the amplitude of the fundamental signal (50 Hz) of current between the first and second tests is studied, where the change of these two values and the extent to which they are affected by the change in the shape of the WS are studied. From this table, it is noted that the THD value increased significantly in the second test for the two controls compared to the first test, as the difference in the THD value between the two tests was estimated at 0.07 and 0.16 for both the DPC-DSTC-MSVM and the DPC-STC, respectively. Therefore, the designed technique provided very little impact compared to the DPC-STC, which indicates the extent of its high performance. This change in the THD value was estimated at 9.75% and 80.4% for both the DPC-STC and the designed DPC-DSTC-MSVM approach, respectively.

TABLE 4. Study of the change in values of fundamental (50 Hz) signal amplitude and current THD between the first and second tests.

		DPC-STC	DPC-DSTC
THD (%)	**Test 1**	1.48	0.80
	Test 2	1.64	0.87
	Test 2 – Test 1	0.16	0.07
	Ratios	9.75%	8.04%
Amplitude of fundamental (50 Hz) signal	**Test 1**	507.20	976.50
	Test 2	504.10	808.50
	Test 2 – Test 1	-3.1	-168
	Ratios	-0.61%	-17.20%

The amplitude of the fundamental signal (50 Hz) decreased significantly in the second test, which indicates that it was affected by the change in the shape of the WS, as the difference in amplitude between the second and third tests was estimated at 3.1 A and 168 A for both the DPC-STC and the proposed DPC-DSTC-MSVM technique, respectively. Therefore, the DPC-DSTC-MSVMprovided the greatest difference compared to the DPC-STC. This difference in amplitude was estimated at 17.20% and 0.61% for both the proposed and DPC-STC strategies, respectively. Through these ratios and this table, the value of THD and the amplitude of the fundamental signal (50 Hz) are greatly affected by the change in WS.

C. TEST_3

This test differs from the above tests, as the same form of WS change used in the second test is used. This test aims to study the robustness of the DPC-DSTC-MSVM compared to the DPC-STC.

In this section, the resistance values will be multiplied by 2 and the inductance values will be divided by 2. Graphical results are displayed in the Fig. 7. Figs. 7a to 7e represent the *Ps*, *Qs*, current, and THD value, respectively. These figures also show that changing the parameters affects both the power and the THD value significantly. This effect is greater if the DPC-STC approach is used compared to DPC-DSTC-MSVM. Also, the power continues to follow the references well despite the change in these parameters, as the value of the *Ps* remains negative and changes according to the change in WS (Fig. 7b). The value of the *Qs* does not change according to the change in WS, as it remains constant and equal to the value 0 VAR in the presence of ripples (Fig. 7c). It is noted that the power fluctuations are less in the case of using the DPC-DSTC-MSVM compared to the DPC-STC, which is a good thing that shows the robustness of the DPC-DSTC-MSVM and its ability to improve the characteristics of the studied system.

Fig. 7d represents the current change profile for the two controls. Despite the change in the system parameters, the current remains sinusoidal for the two controls, with a rise in fluctuations, as these fluctuations are large in the case of using the DPC-STC compared to the DPC-DSTC-MSVM. The value of this current also keeps changing according to the change in WS, which is the same as the observations found in the previous two tests.

In Figs. 7e and 7f, the values of both the THD and the amplitude of the fundamental signal (50Hz) are given for the two controls. Through these two forms, the THD value was 1.72% and 0.93% for both the DPC-STC and DPC-DSTC-MSVM strategies, respectively. So, the DPC-DSTC-MSVM significantly reduced the value of THD, as this reduction was estimated at an estimated rate of 45.93% compared to the DPC-STC. The amplitude value of the fundamental signal (50Hz) was 505 A and 807.80 A for both the DPC-STC and the DPC-DSTC-MSVM, respectively. From these values, the DPC-DSTC-MSVM provided a greater range than the

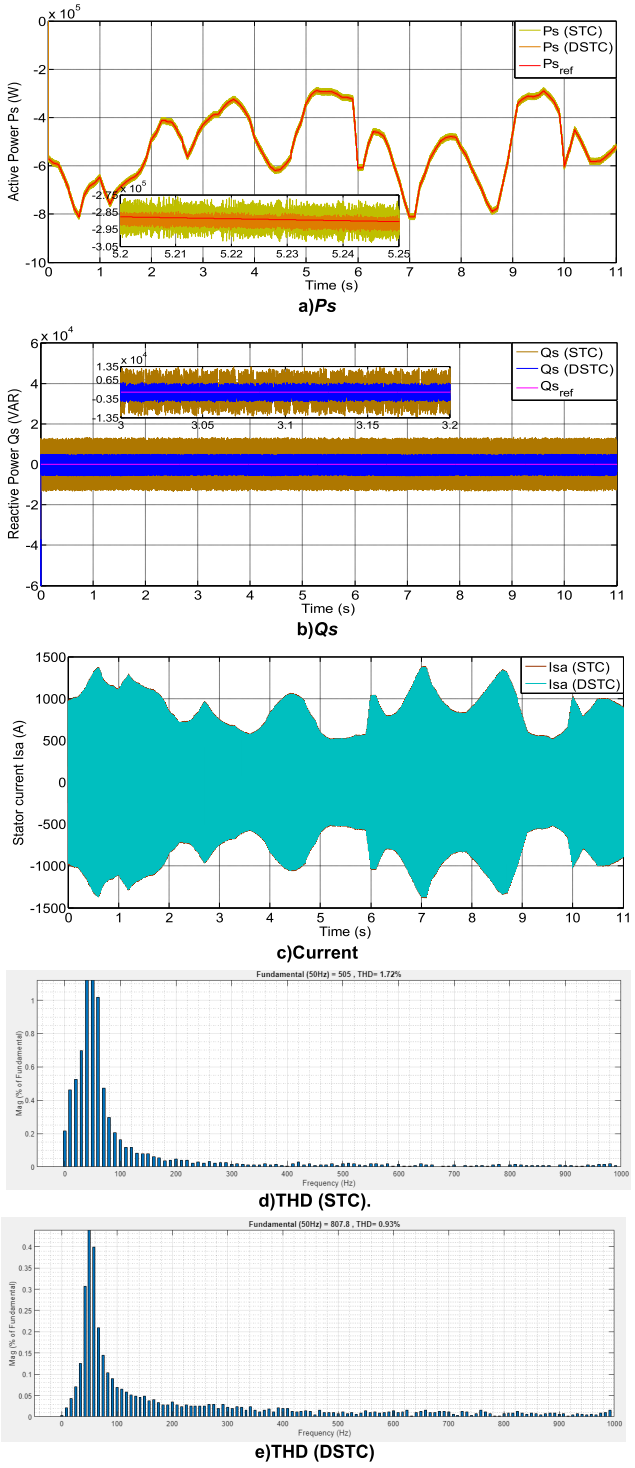

FIGURE 7. Results of the third test.

DPC-STC method by an estimated percentage of 37.48% compared to the DPC-STC. These percentages show that the quality of the current is better if the proposed DPC-DSTC-MSVM is used despite changing the system parameters, which indicates its high robustness compared to the DPC-STC method.

The numerical values for SSE, ripples, RT, and overshoot of DFIG power for the two controls are listed in Table 5, where it is noted that DPC-DSTC-MSVM provided better numerical values than the DPC-STC in terms of ripples, overshoot, and SSE. But in terms of RT capabilities, it provided unsatisfactory results compared to the DPC-STC. Accordingly, the DPC-DSTC-MSVM reduced the values of ripples, overshoot, and SSE of *Qs* by percentages estimated at 59.66%, 59.79%, and 70.60%, respectively, compared to the DPC-STC. The values of fluctuations, overshoot, and SSE of *Ps* were reduced by percentages estimated at 44.88%, 67.34%%, and 70.30%, respectively, compared to the DPC-STC. These calculated percentages indicate the high performance of the DPC-DSTC-MSVM despite the change in system parameters, which is desirable. The DPC-STC reduced the RT to potentials by percentages estimated at 46.30% and 46.72% for *Qs* and *Ps*, respectively, compared to the DPC-STC. Therefore, the response RT to the capabilities is considered to be negative of the designed technique in all tests, as this time can be improved in the future by adding other strategies to the DPC-DSTC-MSVM.

TABLE 5. Numerical results for the third test.

		Ps (W)	*Qs* (VAR)
DPC-STC	Ripples	12700	12100
	Overshoot	2450	1430
	SSE	2290	1395
	RT	0.65 ms	0.8 ms
DPC-DSTC	Ripples	7000	4880
	Overshoot	800	575
	SSE	680	410
	RT	1.22 ms	1.49 ms
Improvement ratios	Ripples	44.88%	59.66%
	Overshoot	67.34%	59.79%
	SSE	70.30%	70.60%
	RT	-46.72%	-46.30%

In Table 6, the change in the values of THD and fundamental (50 Hz) of current for the two commands between the second and third tests is studied. Through this table, the value of THD increased in the third test compared to the second test, as the value of the difference between the two tests was estimated at 0.06% and 0.08% for both the

TABLE 6. Study of the change in values of fundamental (50 Hz) signal amplitude and THD of current between the third and second tests.

		DPC-STC	DPC-DSTC
THD (%)	**Test 2**	1.64	0.87
	Test 3	1.72	0.93
	Test 3 – Test 2	0.08	0.06
	Ratios	4.65%	6.45%
Amplitude of fundamental (50 Hz) signal	**Test 2**	504.10	808.50
	Test 3	505	807.80
	Test 3 – Test 2	0.90	-0.70
	Ratios	0.17%	-0.08%

DPC-DSTC-MSVM technique and the DPC-STC, respectively. Therefore, the DPC-DSTC-MSVM technique provided less difference compared to the DPC-STC. This difference in the THD value was estimated at 6.45% and 4.65% for both the proposed DPC-DSTC-MSVM approach and the DPC-STC, respectively.

In the DPC-STC technique, it is noted that the amplitude of the fundamental signal (50Hz) increased in the third test by 0.90 A compared to the second test. This increase was estimated at 0.17%. However, in the DPC-DSTC-MSVM, this amplitude decreased in the third test by 0.70 A compared to the second test. This decrease in amplitude was estimated at a rate of 0.08%. Therefore, the value of THD and the amplitude of the fundamental signal (50 Hz) are greatly affected by changing system parameters, as the DPC-DSTC-MSVM approach presented a much lower effect than the DPC-STC approach, which indicates its high robustness.

In Table 7, the change in the values of each of the fluctuations, SSE, overshoot, and RT for the two controls is studied during the three tests performed in order to find out which approach provided the least effect.

TABLE 7. Study of the change in the values of ripple, response time, overshoot, and SSE in the three tests.

				DPC-STC	DPC-DSTC
Ripples	*Ps*	Test 1		12000	5000
		Test 2		12500	6800
		Test 3		12700	7000
		Ratios	Test 2-Test 1	4%	26.47%
			Test 3-Test 2	1.57%	2.85%
	Qs	Test 1		12200	3750
		Test 2		11900	4850
		Test 3		12100	4880
		Ratios	Test 2-Test 1	-2.45%	22.68%
			Test 3-Test 2	1.65%	0.61%
SSE	*Ps*	Test 1		2175	750
		Test 2		2250	600
		Test 3		2290	680
		Ratios	Test 2-Test 1	3.33%	-20%
			Test 3-Test 2	1.74%	11.76%
	Qs	Test 1		1250	400
		Test 2		1325	380
		Test 3		1395	410
		Ratios	Test 2-Test 1	5.66%	-5
			Test 3-Test 2	5.01%	7.50%
Overshoot	*Ps*	Test 1		2350	880
		Test 2		2400	700
		Test 3		2450	800
		Ratios	Test 2-Test 1	2.08%	-20.45%
			Test 3-Test 2	2.04%	12.50
	Qs	Test 1		1340	650
		Test 2		1400	520
		Test 3		1430	575
		Ratios	Test 2-Test 1	4.28%	-20%
			Test 3-Test 1	2.09%	9.56%

Table 7 shows that the *Ps* ripples increased in the second test compared to the first test for the two controls, where this increase was estimated at percentages of 4% and 26.47% for both the DPC-STC and the DPC-DSTC-MSVM, respectively. Also, these fluctuations increased in the third test compared to the second test as a result of changing the system parameters, as this increase was estimated at rates of 1.57% and 2.85% for both the DPC-STC and DPC-DSTC-MSVM strategies, respectively. Therefore, the DPC-DSTC-MSVM provided greater rates of change in *Ps* fluctuations than the DPC-STC.

Reactive power fluctuations in the case of the DPC-STC decreased in the second test compared to the first test, and in the case of the DPC-DSTC-MSVM, these fluctuations increased in the second test compared to the first test. This change in the *Qs* fluctuations was estimated at -2.45% and 22.68% for both the DPC-STC and the DPC-DSTC-MSVM, respectively. However, these fluctuations increased in the third test compared to the second test for the two controls, where this increase was estimated at rates of 1.65% and 0.61% for both the DPC-STC and DPC-DSTC-MSVM strategies, respectively. Accordingly, the proposed approach provided a greater percentage of *Qs* ripples in the event of a change in the shape of the WS compared to the DPC-STC, and a smaller percentage in the event of a change in the system parameters.

The SSE values of DFIG power changed in the three tests, which indicates that the SSE value is affected by both the change in the shape of the WS and the values of the system parameters. The SSE value of *Qs* in the case of the DPC-STC increased in the second test compared to the first test and in the third test compared to the second test, where this increase was estimated at percentages of 5.66% and 5.01% for both test 2 - test 1 and test 3 - test 2, respectively. The same observation was observed for the *Ps* in the case of the DPC-STC, where this increase in the SSE value was estimated at rates estimated at 3.33% and 1.74% for test 2 - test 1 and test 3 - test 1, respectively. In the case of the DPC-DSTC-MSVM, the SSE value of DFIG power decreased in the test 2 compared to the test 1, which is a good thing, as this decrease was estimated at 20% and 5% percentages for *Ps* and *Qs*, respectively. However, it is noted that the SSE value of the powers increased in test 3 compared to test 2, and this increase is due to the change in system parameters, as the SSE value was estimated to increase in test 3 compared to test 2 by percentages of 11.76% and 7.50% for *Ps* and *Qs*, respectively. It is also noted that the Overshoot value of the powers in the case of the two controls was affected by changing the shape of the WS and changing the parameter values, as shown in Table 7 for the two commands. In the case of the DPC-STC, the overshoot value increased in the second test compared to the first test, as this increase was estimated at rates of 2.08% and 4.28% for *Ps* and *Qs*, respectively. The overshoot value increased in the third test compared to the second test by percentages estimated at 2.04% and 2.09% for *Ps* and *Qs*, respectively. In the case of the DPC-DSTC-MSVM,

the overshoot value of capabilities decreased in the second test compared to the first test, as this decrease was estimated at percentages of 20.45% and 20% for *Ps* and *Qs*, respectively. However, the third test, presented a higher value for overshoot compared to the second test, where this increase was estimated at 12.50% and 9.56% for *Ps* and *Qs*, respectively.

The designed technique reduced the THD of the supplied currents compared to other commands (Table 8). Based on this table, it can be said that the proposed DPC-DSTC-MSVM can significantly improve the value of THD of current compared to several research works, which makes the quality of the current high if this proposed approach is used, which is a good thing that approaches one of the most prominent solutions in the future. In the field of controlling electrical machines.

TABLE 8. Comparison in terms of THD with other works.

References			THD (%)
[40]		DPC-STA	1.66
[41]		Two-level DTC	8.75
		Three-level DTC	1.57
[42]		SMC	2.56
		High-order SMC	1.08
[43]		ISMC	9.71
		Multi-resonant-based SMC	3.14
[44]		DFOC	2.94
		DFOC-TOSMC	1.42
[14]	DPC-BC	With harmonics suppression strategy	4.59
		Without harmonics suppression strategy	18.51
[45]		DTC-PI	12
		DTC-ACO	7.19
[46]		Predictive torque control	1.73
[47]		Fuzzy DTC	2.40
[48]		DPC-PSO	1.28
[49]		Neural DTC	3.26
[50]		Sliding-backstepping mode control	1.19
DPC-DSTC-MSVM		Test 1	0.80
		Test 2	0.87
		Test 3	0.93

The DPC-DSTC-MSVM is compared with some works in terms of the minimization ratios of undulations, overshoot, and SSE of *Qs* and *Ps*. The comparison results are listed in Tables 9 to 11, where it is noted that the DPC-DSTC-MSVM provided high rates of undulations, overshoot, and SSE of *Ps* and *Qs* compared to some existing commands. So, it can be said that the DPC-DSTC-MSVM has high characteristics and great robustness in improving the efficiency of the systems, and therefore it can be relied upon as a solution in the field of command. Also, the DPC-DSTC-MSVM was compared in terms of response time to potentials with several existing strategies. This comparison is listed in Table 12, where it is noted that the designed approach has good times compared to

TABLE 9. Comparison in terms of SSE for DFIG energy.

Ref.		SSE ratios	
		Qs	*Ps*
[51]		36.93%	35%
[52]		35.48%	62%
[53]		42.14%	47.57%
[54]	Test 1	78.44%	45.83%
	Test 2	52.22%	56.52%
	Test 3	48.75%	87.50%
[55]	Test 1	46.86%	63.96%
	Test 2	45.48%	78%
	Test 3	43.21%	60.03%
[20]	Test 1	76.55%	28.76%
	Test 2	24.62%	30.48%
[27]	Test 1	38.32%	50%
	Test 2	39.68%	40%
DPC-DSTC-MSVM	Test 1	65.51%	68%
	Test 2	73.33%	71.32%
	Test 3	70.30%	70.60%

TABLE 10. Comparison in terms of undulation minimization ratios.

Ref.			Ratios	
			Qs	*Ps*
[54]	DPC-PD(1+PI)	Test 1	54.25	56.66
		Test 2	46.68	47.50
		Test 3	50.74	50.41
[52]	Intelligent command		35%	36%
[53]	Backstepping command		46.93%	28.57%
[51]			36.93%	22.95%
[56]	DPC-PI(1+PI)	Test 1	50	44.50
		Test 2	52.98	63.33
		Test 3	50	48.18
[57]		Test 1	47.05%	69.33%
		Test 2	47.99%	65.07%
[20]		Test 1	20.66%	37.50%
		Test 2	20.80%	16.66%
[27]		Test 1	12.02%	10%
		Test 2	10.53%	5.88%
DPC-DSTC-MSVM		Test 1	58.33%	69.26%
		Test 2	45.60%	59.24%
		Test 3	44.88%	59.66%

other strategies, which shows the rapid dynamic response that characterizes it. Accordingly, these completed comparisons show the extent of high performance and the effectiveness of the DPC-DSTC-MSVM in improving the values of ripples, response time, overshoot, and SSE of DFIG power, making it one of the most promising solutions that can be relied upon in the future.

VI. HIL TEST OF DSTC STRATEGY

To test the industrial reliability of our DPC-DSTC-MSVM technique, a computer containing the MATLAB 2021b program is used, where the DPC-DSTC-MSVM is implemented and embedded in the dSPACE DS1104 R&D card, which is

TABLE 11. Comparison in terms of overshoot minimization ratios.

Ref.		Ratios	
		Qs	*Ps*
[20]	Test 1	6.44%	25.07%
	Test 2	6.05%	9.19%
[24]		16.59	7.23
[27]	Test 1	44.06%	32.20%
	Test 2	22.77%	32.49%
[58]		60.93	67.74
[52]		37.42%	80%
[53]		60.93%	67.74%
[56]	Test 1	48.38%	73.87%
	Test 2	49.32%	20.10%
DPC-DSTC-MSVM	Test 1	62.55%	51.49%
	Test 2	70.83%	62.85%
	Test 3	67.34%	59.79%

TABLE 12. Comparison in terms of response time of DFIG energy.

References		Response time	
		Ps	*Qs*
[59]		15 ms	80 ms
[60]	DPC	17 ms	18 ms
	Nonlinear DPC method	9 ms	5 ms
[50]		33.8 ms	34.5 ms
[61]	Test 1	1.70 ms	1.85 ms
	Test 2	1.34 ms	1.183 ms
[62]		-	28 ms
[14]		1.50 ms	0.80 ms
[63]	Vector control with additional resonant controller	5 ms	4 ms
[64]	LUT-DPC	2.2 ms	0.90 ms
[10]	Synergetic control	1.78 ms	8.50 ms
[65]	Test 1	0.9 ms	2.10 ms
	Test 2	2.50 ms	3 ms
	Test 3	2.65 ms	3.25 ms
	Test 4	4.80 ms	5.40 ms
[66]	Test 1	12.15 ms	10.08 ms
	Test 2	11.25 ms	9.85 ms
	Test 3	11.85 ms	10.05 ms
[26]	Test 1	3.87 ms	2.58 ms
	Test 2	1.29 ms	0.46 ms
DPC-DSTC-MSVM	Test 1	1.22 ms	1.49 ms
	Test 2	1.23 ms	1.45 ms
	Test 3	0.98 ms	0.89 ms

developed and made by the German company "Dspace GmbH". This embedded system board sends the necessary signals to the IGBT inverter in real time, as shown in Figs. 8 and 9. In addition, the DS1104 regulator board collects from the MRWT system all measurements requested by the DPC-DSTC-MSVM. Figs. 8 and 9 show how the dSPACE controller board communicates with an MRWT based on a DFIG with the use of an IGBT inverter. As part of this project to realize a robust control system, experimental validation, and testing were carried out using a real experimental bench. Experimental tests and validation were carried out using the dSPACE board, the real-time interface (RTI), and the real-time workshop (RTW) tool. Thanks to this research

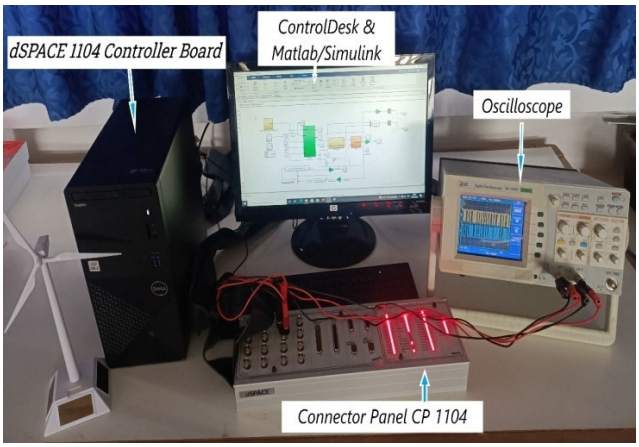

FIGURE 8. HIL test experimental bench of DSTC control.

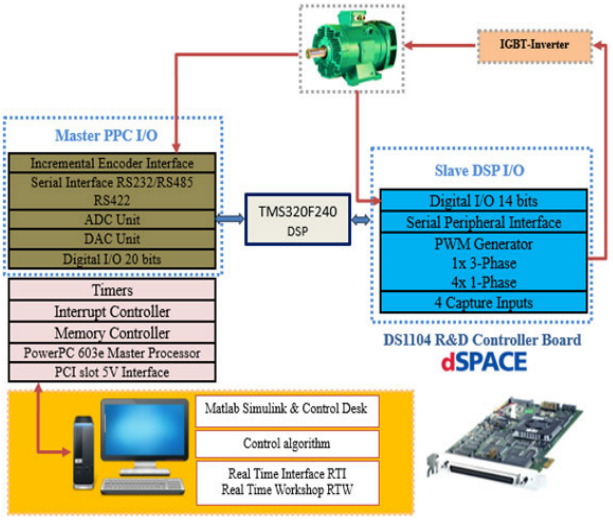

FIGURE 9. Implementation structure of the DPC-DSTC.

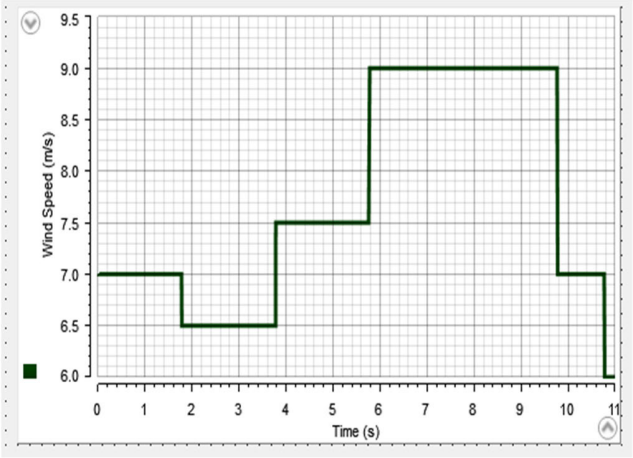

FIGURE 10. Steps WS profile.

work and its experimental realization, it can be said that this command is easy to realize, to implement, low cost, and does not require specialists or effort or a complex program. The DPC-DSTC-MSVM can, therefore, be used more widely in the future by wind energy industrialists.

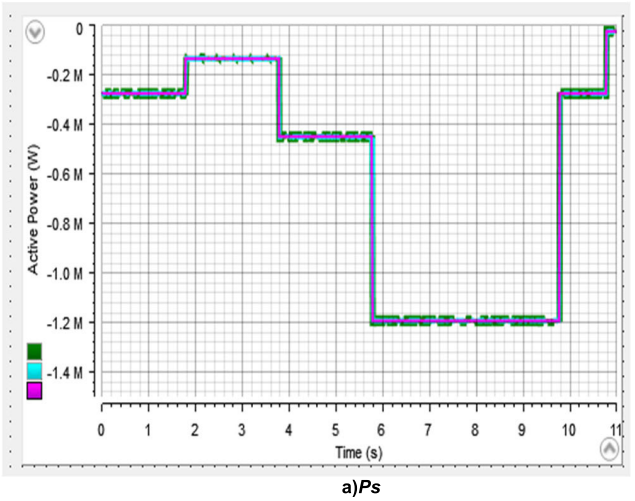

a)*Ps*

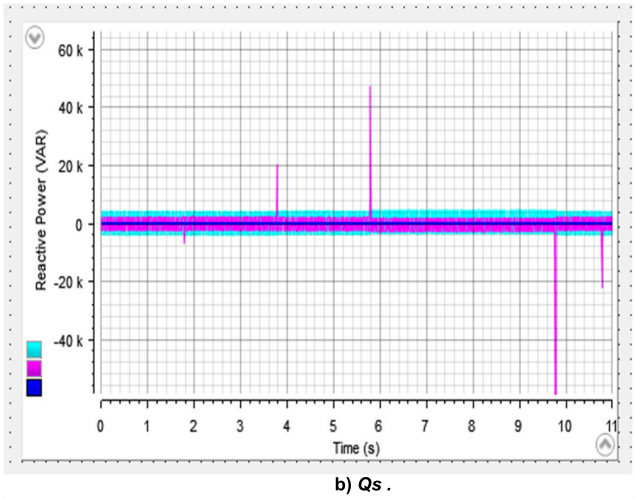

b) *Qs* .

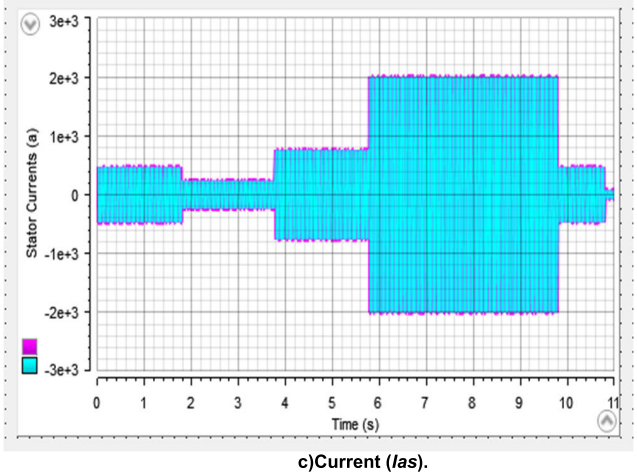

c)Current (*Ias*).

FIGURE 11. Experimental results when using steps WS profile.

The DPC-DTSC-MSVM of DFIG-MRWT was tested experimentally using two different forms of WS, where variable WS and WS in steps were used to study the behavior of the DPC-DSTC-MSVM and compare it with the DPC-STC approach.

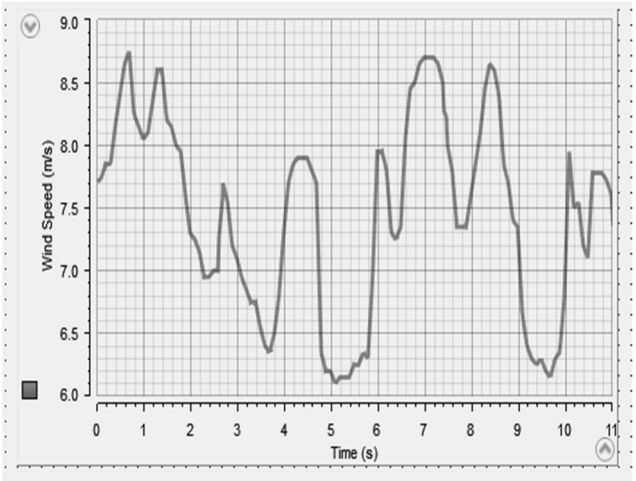

FIGURE 12. Variable WS profile.

First case: Steps WS profile.

First, experimental work is carried out using dSPACE 1104 for the DPC-DSTC-MSVM in the case of WS taking the form of steps. The latter is represented in Fig. 10, where the experimental results in this case are represented in Fig. 11. The latter gives a clear picture of the superiority of the DPC-DSTC-MSVM over the DPC-STC in terms of minimizing undulations. Also, it is noted that the energies track references well, which is the same as the results of Section IV in terms of tracking references and ripples. *Ps* takes the form of a change in WS (Fig. 11a), but *Qs* remain constant and do not change according to a change in WS (Fig. 11b). In Fig. 11c, it is noted that the current changes according to the change in WS. These are the same simulation results with a sinusoidal shape for the current in the two commands.

The second case: Variable WS profile.

The experimental work in the second case is different from the first case, as the difference lies in the kind or form of WS change used to study the behavior of the DPC-DSTC-MSVM compared to the DPC-STC.

The WS used in this second case of experimental work is represented in Fig. 12. The experimental results are represented in Fig. 13, where it is noted at first glance that the experimental results in this case are the same as the numerical results. The *Ps* take the form of a change in WS and follow the reference well, with fewer undulations in the DPC-DSTC-MSVM approach compared to the DPC-STC, and this is what Fig. 13a shows. In Fig. 13b, it is observed experimentally that the *Qs* are not affected by the form of a change in WS and follow reference well. Also, it is noted that the undulations are lower in the DPC-DSTC-MSVM compared to the DPC-STC, which is a positive thing that indicates the superiority of the DPC-DSTC-MSVM. The current for the two strategies is represented in Fig. 13c, where it is noted that the current changes according to the change in WS with a sinusoidal shape, and its value increases according to the increase in WS.

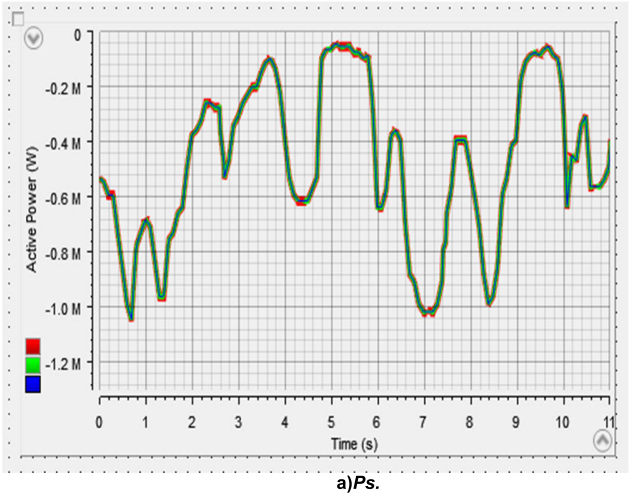

a)*Ps.*

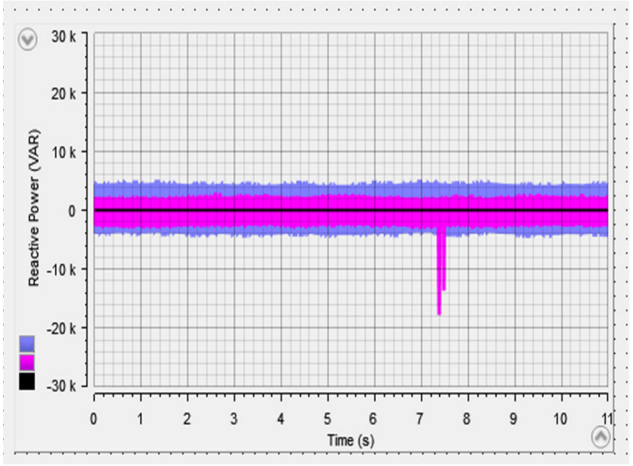

b)*Qs*

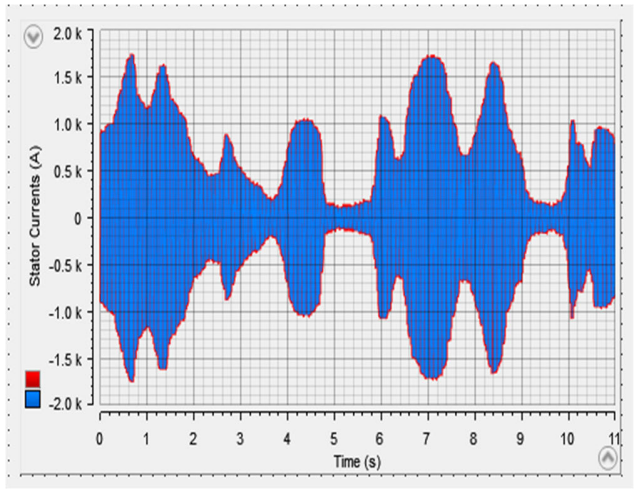

c)Current

FIGURE 13. Experimental results when using variable WS profile.

VII. CONCLUSION

In this new research study, a robust new command is suggested to ameliorate the robustness of the DPC for the DFIG-MRWT systems. The DSTC algorithm is designed to replace the conventional HCs of the DPC. The novel-designed DPC-DSTC-MSVM preserves the characteristics of the DPC such as less parameter dependence and simplicity. The effectiveness and robustness of both strategies are studied under, THD of current and power ripples. By comparing the characteristics of the suggested control scheme with DPC-STC, it can concluded that the DPC-DSTC-MSVM has reduced the current THD. The DPC-DSTC-MSVM has been very successful in improving the current quality provided by the DFIG-MRWT system. Also, the experimental results obtained using the HIL test (dSPACE 1104) show that the DPC-DSTC-MSVM has a distinctive and effective competence in ameliorating the cons of the DFIG-MRWT, as it is noted that the experimental results are almost the same as the simulated results.

In future work, we will try to add intelligent techniques such as grey wolf optimization or NNs to determine the values of the DPC-DSTC-MSVM gains and compare the results with other strategies. In addition, trying to accomplish this work experimentally and apply other new strategies to significantly minimize power undulations.

APPENDIX

Table 13 shows the parameters of the machine used in this work.

TABLE 13. Machine parameters.

Parameter	Values
R_s	12 mΩ
P_{sn}	1500 kW
L_r	13.6 mH
L_m	13.5 mH
p	2
J	1 Mg.m^2
L_s	13.7 mH
R_r	21 mΩ
f_r	2.4 mN.m/s
Vs	380/696 V
fs	50 Hz

REFERENCES

[1] H. Kong, J. He, Y. Liu, P. Cheng, and J. Ma, "Improved direct power control of doubly fed induction generator without phase-locked loop," in *Proc. IEEE Sustain. Power Energy Conf. (iSPEC)*, Jul. 2020, pp. 199–204, doi: 10.1109/ISPEC50848.2020.9351036.

[2] S. M. Tavakoli, M. A. Pourmina, and M. R. Zolghadri, "Comparison between different DPC methods applied to DFIG wind turbines," *Int. J. Renew. Energy Res.*, vol. 3, no. 2, pp. 446–452, 2013, doi: 10.20508/ijrer.v3i2.680.g6162.

[3] V. Mishra, R. Dev Shukla, and P. Gupta, "An approach towards application of semiconductor electronics converter in autonomous DFIM based wind energy generation system: A review," *Int. J. Smart Grid*, vol. 3, no. 3, pp. 152–162, 2019, doi: 10.20508/ijsmartgrid.v3i3.69.g61.

[4] N. Debdouche, H. Benbouhenni, B. Deffaf, G. Anwar, and L. Zarour, "Predictive direct power control with phase-locked loop technique of three-level neutral point clamped inverter based shunt active power filter for power quality improvement," *Int. J. Circuit Theory Appl.*, vol. 52, no. 7, pp. 3306–3340, Jul. 2024, doi: 10.1002/cta.3871.

[5] B. Hu, H. Nian, J. Yang, M. Li, and Y. Xu, "High-frequency resonance analysis and reshaping control strategy of DFIG system based on DPC," *IEEE Trans. Power Electron.*, vol. 36, no. 7, pp. 7810–7819, Jul. 2021, doi: 10.1109/TPEL.2020.3045860.

[6] Z. Zhang, F. Wang, J. Wang, J. Rodríguez, and R. Kennel, "Nonlinear direct control for three-level NPC back-to-back converter PMSG wind turbine systems: Experimental assessment with FPGA," *IEEE Trans. Ind. Informat.*, vol. 13, no. 3, pp. 1172–1183, Jun. 2017, doi: 10.1109/TII.2017.2678500.

[7] F. Mazouz, B. Sebti, and C. Ilhami, "DPC-SVM of DFIG using fuzzy second order sliding mode approach," *Int. J. Smart Grid*, vol. 5, no. 4, pp. 174–182, 2021, doi: 10.20508/ijsmartgrid.v5i4.219.g178.

[8] J. Mohammadi, S. Vaez-Zadeh, S. Afsharnia, and E. Daryabeigi, "A combined vector and direct power control for DFIG-based wind turbines," *IEEE Trans. Sustain. Energy*, vol. 5, no. 3, pp. 767–775, Jul. 2014, doi: 10.1109/TSTE.2014.2301675.

[9] B. Habib, B. Zinelaabidine, and B. Abdelkader, "A direct power control of the doubly fed induction generator based on the three-level NSVPWM technique," *Int. J. Smart Grid*, vol. 3, no. 4, pp. 216–225, 2019, doi: 10.20508/ijsmartgrid.v3i4.86.g74.

[10] A. Ardjal, M. Bettayeb, R. Mansouri, and A. Mehiri, "Nonlinear synergetic control approach for DC-link voltage regulator of wind turbine DFIG connected to the grid," in *Proc. 5th Int. Conf. Renew. Energy: Gener. Appl. (ICREGA)*, Al Ain, United Arab Emirates, Feb. 2018, pp. 94–97, doi: 10.1109/ICREGA.2018.8337639.

[11] M. Pichan, H. Rastegar, and M. Monfared, "Fuzzy-based direct power control of doubly fed induction generator-based wind energy conversion systems," in *Proc. 2nd Int. eConference Comput. Knowl. Eng. (ICCKE)*, Oct. 2012, pp. 66–70, doi: 10.1109/ICCKE.2012.6395354.

[12] G. Kambam, P. Somasundaram, and G. V. Swaminathan, "Design of GSC and RSC controllers for DFIG using GA based optimization algorithm," in *Proc. 9th Int. Conf. Electr. Energy Syst. (ICEES)*, Chennai, India, Mar. 2023, pp. 210–215, doi: 10.1109/ICEES57979.2023.10110288.

[13] J. Hu, H. Nian, B. Hu, Y. He, and Z. Q. Zhu, "Direct active and reactive power regulation of DFIG using sliding-mode control approach," *IEEE Trans. Energy Convers.*, vol. 25, no. 4, pp. 1028–1039, Dec. 2010, doi: 10.1109/TEC.2010.2048754.

[14] P. Xiong and D. Sun, "Backstepping-based DPC strategy of a wind turbine-driven DFIG under normal and harmonic grid voltage," *IEEE Trans. Power Electron.*, vol. 31, no. 6, pp. 4216–4225, Jun. 2016, doi: 10.1109/TPEL.2015.2477442.

[15] S. Boubzizi, H. Abid, A. El Hajjaji, and M. Chaabane, "Comparative study of three types of controllers for DFIG in wind energy conversion system," *Protection Control Modern Power Syst.*, vol. 3, no. 3, pp. 1–12, Jul. 2018, doi: 10.1186/s41601-018-0096-y.

[16] H. Dong, M. Su, K. Liu, and W. Zou, "Mitigation strategy of subsynchronous oscillation based on fractional-order sliding mode control for VSC-MTDC systems with DFIG-based wind farm access," *IEEE Access*, vol. 8, pp. 209242–209250, 2020, doi: 10.1109/ACCESS.2020.3038665.

[17] H. Benbouhenni, "Utilization of an ANFIS-STSM algorithm to minimize total harmonic distortion," *Int. J. Smart Grid*, vol. 4, no. 2, pp. 56–67, 2020.

[18] M. Yessef, M. Taoussi, H. Benbouhenni, A. Lagrioui, I. Colak, H. Ameziane, B. Majout, and B. Bossoufi, "Two different controllers-based DPC of the doubly-fed induction generator with real-time implementation on dSPACE 1104 controller board," *Meas. Control*, pp. 1–23, Feb. 2024, doi: 10.1177/00202940241236288.

[19] I. Sami, S. Ullah, S. U. Amin, A. Al-Durra, N. Ullah, and J.-S. Ro, "Convergence enhancement of super-twisting sliding mode control using artificial neural network for DFIG-based wind energy conversion systems," *IEEE Access*, vol. 10, pp. 97625–97641, 2022, doi: 10.1109/ACCESS.2022.3205632.

[20] H. Benbouhenni, N. Bizon, and I. Colak, "Super-twisting hysteresis controller for multi-rotor wind energy systems," *Int. J. Electron.*, pp. 1–20, Feb. 2024, doi: 10.1080/00207217.2024.2312086.

[21] H. Benbouhenni and H. Gasmi, "Comparative study of synergetic controller with super twisting algorithm for rotor side inverter of DFIG," *Int. J. Smart Grid*, vol. 6, no. 4, pp. 144–156, 2022, doi: 10.20508/ijsmartgrid.v6i4.265.g251.

[22] N. K. Mishra and Z. Husain, "Application of novel six-phase doubly fed induction generator for open phases through modeling and simulation," *IETE J. Res.*, vol. 69, no. 6, pp. 3916–3927, Aug. 2023, doi: 10.1080/03772063.2021.1933627.

[23] N. Debdouche, B. Deffaf, H. Benbouhenni, Z. Laid, and M. I. Mosaad, "Direct power control for three-level multifunctional voltage source inverter of PV systems using a simplified super-twisting algorithm," *Energies*, vol. 16, no. 10, p. 4103, May 2023, doi: 10.3390/en16104103.

[24] I. Sami, S. Ullah, Z. Ali, N. Ullah, and J.-S. Ro, "A super twisting fractional order terminal sliding mode control for DFIG-based wind energy conversion system," *Energies*, vol. 13, no. 9, p. 2158, May 2020, doi: 10.3390/en13092158.

[25] H. Gasmi, S. Mendaci, S. Laifa, W. Kantas, and H. Benbouhenni, "Fractional-order proportional-integral super twisting sliding mode controller for wind energy conversion system equipped with doubly fed induction generator," *J. Power Electron.*, vol. 22, no. 8, pp. 1357–1373, Aug. 2022, doi: 10.1007/s43236-022-00430-0.

[26] A. Yahdou, A. B. Djilali, E. Bounadja, and H. Benbouhenni, "Using neural network super-twisting sliding mode to improve power control of a dual-rotor wind turbine system in normal and unbalanced grid fault modes," *Int. J. Circuit Theory Appl.*, pp. 1–25, Feb. 2024, doi: 10.1002/cta.3960.

[27] M. Yessef, H. Benbouhenni, M. Taoussi, A. Lagrioui, I. Colak, S. Mobayen, A. Zhilenkov, and B. Bossoufi, "Real-time validation of intelligent super-twisting sliding mode control for variable-speed DFIG using dSPACE 1104 board," *IEEE Access*, vol. 12, pp. 31892–31915, 2024, doi: 10.1109/ACCESS.2024.3367828.

[28] H. Benbouhenni, L.-M. Ionescu, A.-G. Mazare, D. Zellouma, I. Colak, and N. Bizon, "Active and reactive power vector control using neural-synergetic-super twisting controllers of induction generators for variable-speed contra-rotating wind turbine systems," *Meas. Control*, vol. 57, no. 7, pp. 919–948, Jul. 2024, doi: 10.1177/00202940231224386.

[29] H. Benbouhenni, M. Yessef, I. Colak, N. Bizon, H. Kotb, K. M. AboRas, and A. Elrashidi, "Dynamic performance of rotor-side nonlinear control technique for doubly-fed multi-rotor wind energy based on improved super-twisting algorithms under variable wind speed," *Sci. Rep.*, vol. 14, no. 1, pp. 1–24, Mar. 2024, doi: 10.1038/s41598-024-55271-7.

[30] R. Ryndzionek, K. Blecharz, F. Kutt, M. Michna, and G. Kostro, "Fault-tolerant performance of the novel five-phase doubly-fed induction generator," *IEEE Access*, vol. 10, pp. 59350–59358, 2022, doi: 10.1109/ACCESS.2022.3179815.

[31] N. K. Mishra, G. Mishra, and M. K. Shukla, "Six-phase DFIG-MPPT synergy: Pioneering approaches for maximising energy yield in wind energy generation system," *Int. J. Power Energy Convers.*, vol. 15, no. 1, pp. 79–98, 2024, doi: 10.1504/ijpec.2024.136854.

[32] Z. Heidari, H. Gorginpour, and M. Shahparasti, "Optimal electromagnetic-thermal design of a seven-phase induction motor for high-power speed-control applications," *Trans. Comput. Sci. Eng. Elect. Eng. (D)*, vol. 29, no. 5, pp. 2480–2497, 2022, doi: 10.24200/SCI.2021.54766.4028.

[33] L. Fang, D. Li, and R. Qu, "Torque improvement of Vernier permanent magnet machine with larger rotor pole pairs than stator teeth number," *IEEE Trans. Ind. Electron.*, vol. 70, no. 12, pp. 12648–12659, Dec. 2023, doi: 10.1109/TIE.2022.3232651.

[34] H. Benbouhenni, F. Mehedi, and L. Soufiane, "New direct power synergetic-SMC technique based PWM for DFIG integrated to a variable speed dual-rotor wind power," *Automatika*, vol. 63, no. 4, pp. 718–731, Dec. 2022, doi: 10.1080/00051144.2022.2065801.

[35] H. Benbouhenni, N. Bizon, I. Colak, P. Thounthong, and N. Takorabet, "Simplified super twisting sliding mode approaches of the double-powered induction generator-based multi-rotor wind turbine system," *Sustainability*, vol. 14, no. 9, p. 5014, Apr. 2022, doi: 10.3390/su14095014.

[36] A. Yahdou, B. Hemici, and Z. Boudjema, "Second order sliding mode control of a dual-rotor wind turbine system by employing a matrix converter," *J. Electr. Eng.*, vol. 16, pp. 1–11, Jan. 2016.

[37] B. Habib, "Application of STA methods and modified SVM strategy in direct vector control system of ASG integrated to dual-rotor wind power: Simulation studies," *Int. J. Smart Grid*, vol. 5, no. 1, pp. 63–73, 2021, doi: 10.20508/ijsmartgrid.v5i1.173.g136.

[38] B. Habib, N. Bizon, and I. Colak, "A brief review of space vector modulation (SVM) methods and a new SVM technique based on the minimum and maximum of the three-phase voltages," *Iranian J. Electr. Electron. Eng.*, vol. 18, no. 3, pp. 1–18, 2022, doi: 10.22068/IJEEE.18.3.2358.

[39] B. Habib, "Stator current and rotor flux ripples reduction of DTC DFIG drive using FSTSMC algorithm," *Int. J. Smart Grid*, vol. 3, no. 4, pp. 226–234, 2019, doi: 10.20508/ijsmartgrid.v3i4.82.g72.

[40] I. Yaichi, A. Semmah, P. Wira, and Y. Djeriri, "Super-twisting sliding mode control of a doubly-fed induction generator based on the SVM strategy," *Periodica Polytechnica Electr. Eng. Comput. Sci.*, vol. 63, no. 3, pp. 178–190, Jun. 2019.

[41] N. El Ouanjli, A. Derouich, A. El Ghzizal, M. Taoussi, Y. El Mourabit, K. Mezioui, and B. Bossoufi, "Direct torque control of doubly fed induction motor using three-level NPC inverter," *Protection Control Modern Power Syst.*, vol. 4, no. 3, pp. 1–9, Jul. 2019, doi: 10.1186/s41601-019-0131-7.

[42] K. D. Eddine, A. Mezouar, L. Boumediene, and A. P. M. Van Den Bossche, "A comprehensive review of LVRT capability and sliding mode control of grid-connected wind-turbine-driven doubly fed induction generator," *Automatika*, vol. 57, no. 4, pp. 922–935, Oct. 2016, doi: 10.7305/automatika.2017.05.1813.

[43] Y. Quan, L. Hang, Y. He, and Y. Zhang, "Multi-resonant-based sliding mode control of DFIG-based wind system under unbalanced and harmonic network conditions," *Appl. Sci.*, vol. 9, no. 6, p. 1124, Mar. 2019, doi: 10.3390/app9061124.

[44] H. Benbouhenni and N. Bizon, "A synergetic sliding mode controller applied to direct field-oriented control of induction generator-based variable speed dual-rotor wind turbines," *Energies*, vol. 14, no. 15, p. 4437, Jul. 2021, doi: 10.3390/en14154437.

[45] S. Mahfoud, A. Derouich, A. Iqbal, and N. El Ouanjli, "ANT-colony optimization-direct torque control for a doubly fed induction motor : An experimental validation," *Energy Rep.*, vol. 8, pp. 81–98, Nov. 2022, doi: 10.1016/j.egyr.2021.11.239.

[46] M. A. Mossa, H. Echeikh, and A. Iqbal, "Enhanced control technique for a sensor-less wind driven doubly fed induction generator for energy conversion purpose," *Energy Rep.*, vol. 7, pp. 5815–5833, Nov. 2021.

[47] W. Ayrir, M. Ourahou, B. El Hassouni, and A. Haddi, "Direct torque control improvement of a variable speed DFIG based on a fuzzy inference system," *Math. Comput. Simul.*, vol. 167, pp. 308–324, Jan. 2020, doi: 10.1016/j.matcom.2018.05.014.

[48] B. Mohamed Rida, M. Rahli, S. Slami, and L. Hassaine, "PSO based direct power control for a multifunctional grid connected photovoltaic system," *Int. J. Power Electron. Drive Syst. (IJPEDS)*, vol. 9, no. 2, p. 610, Jun. 2018.

[49] M. Said, A. Derouich, N. El Ouanjli, and M. El Mahfoud, "Enhancement of the direct torque control by using artificial neuron network for a doubly fed induction motor," *Intell. Syst. Appl.*, vol. 13, pp. 1–18, Jul. 2022, doi: 10.1016/j.iswa.2022.200060.

[50] F. Echiheb, Y. Ihedrane, B. Bossoufi, M. Bouderbala, S. Motahhir, M. Masud, S. Aljahdali, and M. ElGhamrasni, "Robust sliding-backstepping mode control of a wind system based on the DFIG generator," *Sci. Rep.*, vol. 12, no. 1, p. 11782, Jul. 2022, doi: 10.1038/s41598-022-15960-7.

[51] H. Benbouhenni, H. Gasmi, I. Colak, N. Bizon, and P. Thounthong, "Synergetic-PI controller based on genetic algorithm for DPC-PWM strategy of a multi-rotor wind power system," *Sci. Rep.*, vol. 13, no. 1, pp. 1–20, Aug. 2023, doi: 10.1038/s41598-023-40870-7.

[52] B. Habib, H. Gasmi, and I. Colak, "Intelligent control scheme of asynchronous generator-based dual-rotor wind power system under different working conditions," *Majlesi J. Energy Manag.*, vol. 11, no. 3, pp. 8–15, 2022. [Online]. Available: https://em.majlesi.info/index.php/em/article/view/494

[53] H. Benbouhenni, H. Gasmi, and I. Colak, "Backstepping control for multi-rotor wind power systems," *Majlesi J. Energy Manage.*, vol. 11, no. 4, pp. 8–15, 2023. [Online]. Available: https://em.majlesi.info/index.php/em/article/view/493

[54] H. Benbouhenni, E. Bounadja, H. Gasmi, N. Bizon, and I. Colak, "A new PD(1+PI) direct power controller for the variable-speed multi-rotor wind power system driven doubly-fed asynchronous generator," *Energy Rep.*, vol. 8, pp. 15584–15594, Nov. 2022, doi: 10.1016/j.egyr.2022.11.136.

[55] H. Benbouhenni, I. Colak, N. Bizon, A. G. Mazare, and P. Thounthong, "Direct vector control using feedback PI controllers of a DPAG supplied by a two-level PWM inverter for a multi-rotor wind turbine system," *Arabian J. Sci. Eng.*, vol. 48, no. 11, pp. 15177–15193, Nov. 2023, doi: 10.1007/s13369-023-08035-w.

[56] H. Benbouhenni, D. Zellouma, N. Bizon, and I. Colak, "A new PI(1 +PI) controller to mitigate power ripples of a variable-speed dual-rotor wind power system using direct power control," *Energy Rep.*, vol. 10, pp. 3580–3598, Nov. 2023, doi: 10.1016/j.egyr.2023.10.007.

[57] H. Benbouhenni, N. Bizon, P. Thounthong, I. Colak, and P. Mungporn, "A new integral-synergetic controller for direct reactive and active powers control of a dual-rotor wind system," *Meas. Control*, vol. 57, no. 2, pp. 208–224, Feb. 2024, doi: 10.1177/00202940231195117.

[58] H. Benbouhenni, "Comparative study of sliding mode control with synergetic control for rotor side inverter of the DFIG for multi-rotor wind power systems," *Majlesi J. Mechatron. Syst.*, vol. 11, no. 2, pp. 29–37, 2023. [Online]. Available: https://ms.majlesi.info/index.php/ms/article/view/532

[59] H. E. Alami, B. Bossoufi, S. Motahhir, E. H. Alkhammash, M. Masud, M. Karim, M. Taoussi, M. Bouderbala, M. Lamnadi, and M. El Mahfoud, "FPGA in the loop implementation for observer sliding mode control of DFIG-generators for wind turbines," *Electronics*, vol. 11, no. 1, p. 116, Dec. 2021, doi: 10.3390/electronics11010116.

[60] Y. Ibrahim, A. Semmah, and W. Patrice, "Neuro-second order sliding mode control of a DFIG based wind turbine system," *J. Electr. Electron. Eng.*, vol. 13, no. 1, pp. 63–68, 2020.

[61] M. Yessef, H. Benbouhenni, M. Taoussi, A. Lagrioui, I. Colak, B. Bossoufi, and T. A. H. Alghamdi, "Experimental validation of feedback PI controllers for multi-rotor wind energy conversion systems," *IEEE Access*, vol. 12, pp. 7071–7088, 2024, doi: 10.1109/ACCESS.2024.3351355.

[62] C. Hamid, D. Aziz, C. S. Eddine, Z. Othmane, T. Mohammed, and E. Hasnae, "Integral sliding mode control for DFIG based WECS with MPPT based on artificial neural network under a real wind profile," *Energy Reports*, vol. 7, pp. 4809–4824, Nov. 2021, doi: 10.1016/j.egyr.2021.07.066.

[63] C. J. Ramos, A. P. Martins, and A. S. Carvalho, "Rotor current controller with voltage harmonics compensation for aDFIG operating under unbalanced and distorted stator voltage," in *Proc. 33rd Annu. Conf. IEEE (IECON)*, 2007, pp. 5–8.

[64] F. Wei, X. Zhang, D. M. Vilathgamuwa, S. S. Choi, and S. Wang, "Mitigation of distorted and unbalanced stator voltage of stand-alone doubly fed induction generators using repetitive control technique," *IET Electric Power Appl.*, vol. 7, no. 8, pp. 654–663, Sep. 2013.

[65] A. Yahdou, H. Benbouhenni, I. Colak, and N. Bizon, "Application of backstepping control with nonsingular terminal sliding mode surface technique to improve the robustness of stator power control of asynchronous generator-based multi-rotor wind turbine system," *Electric Power Compon. Syst.*, pp. 1–29, Jan. 2024, doi: 10.1080/15325008.2024.2304688.

[66] H. Benbouhenni, M. Yessef, N. Bizon, S. Kadi, B. Bossoufi, and A. Alhejji, "Hardware-in-the-loop simulation to validate the fractional-order neuro-fuzzy power control of variable-speed dual-rotor wind turbine systems," *Energy Rep.*, vol. 11, pp. 4904–4923, Jun. 2024, doi: 10.1016/j.egyr.2024.04.049.

HABIB BENBOUHENNI was born in Chlef, Algeria. He received the M.A. degree in automatic and industrial informatics, in 2017, and the Ph.D. degree in electrical engineering from ENPO-MA, Oran, Algeria. He is currently a Professor with the University of Nisantasi, Turkey. His research interest includes the application of robust control in wind turbine power systems. He is an editor of seven books and more than 250 articles in scientific fields related to electrical engineering. In recent years, he has served as a Committee Member for several scientific conferences, such as ECAI-2024 and ECA-2023. He is also a Committee Member of *Symmetry* and EPCS journals.

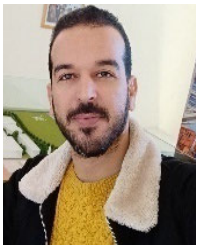

MOURAD YESSEF was born in Taounate, Morocco. He received the master's degree in sciences and technology titled "microelectronic" from the Faculty of Sciences, Sidi Mohamed Ben Abdallah University, Fes, Morocco. He is currently pursuing the joint Ph.D. degree in electrical engineering with the Faculty of Sciences, Sidi Mohamed Ben Abdallah University, and Higher National School of Arts and Trades (ENSAM-Meknes), Moulay Ismail University, Meknes, Morocco. His research interests include renewable energy, smart grids, artificial intelligence, embedded systems, control systems, and power electronics.

NICU BIZON (Senior Member, IEEE) was born in Albesti de Muscel, Arges, Romania, in 1961. He received the B.S. degree in electronic engineering and the Ph.D. degree in automatic systems and control from the University Polytechnic of Bucharest, Romania, in 1986 and 1996, respectively. From 1996 to 1989, he was in hardware design with Dacia Renault SA, Romania. He is currently a Professor with the University of Pitesti, Romania. His current research interests include power electronic converters, fuel cell and electric vehicles, renewable energy, energy storage systems, microgrids, and control and optimization of these systems. He received two awards from Romanian Academy, in 2013 and 2016. He is an editor of ten books and more than 500 articles in scientific fields related to energy.

BADRE BOSSOUFI was born in Fes, Morocco, in 1985. He received the Ph.D. degree in electrical engineering from the Faculty of Sciences, University Sidi Mohammed Ben Abdellah, Fes, and the joint Ph.D. degree from the Faculty of Electronics and Computer, University of Pitesti, Romania, and Montefiore Institute of Electrical Engineering, Luik, Belgium, in 2012. He is currently a Professor in electrical engineering with the Faculty of Sciences, Sidi Mohamed Ben Abdellah University. He has published more than 134 journals and conference papers indexed Scopus and/or Web of Sciences (WoS). He named one of the top 2% scientists worldwide 2023 by Stanford University. His research interests include static converters, electrical motor drives, power electronics, smart grids, renewable energy, and artificial intelligence.

THAMER A. H. ALGHAMDI received the B.Sc. degree from Al-Baha University, Al Bahah, Saudi Arabia, in 2012, the M.Sc. degree from Northumbria Newcastle University, Newcastle, U.K., in 2016, and the Ph.D. degree from Cardiff University, Cardiff, U.K., in 2023. He is currently an Assistant Professor in electrical power engineering with Al-Baha University. He was a Power Distribution Engineer with Saudi Electricity Company (SEC), until 2013. He was a Lecturer Assistant with Al-Baha University, from 2016 to 2018. His main research interests include power systems, power quality, the integration of renewables, and AI applications in electrical engineering.